Cell Reports

Article

An *in situ* analysis pipeline for initial host-pathogen interactions reveals signatures of human colorectal HIV transmission

Graphical abstract

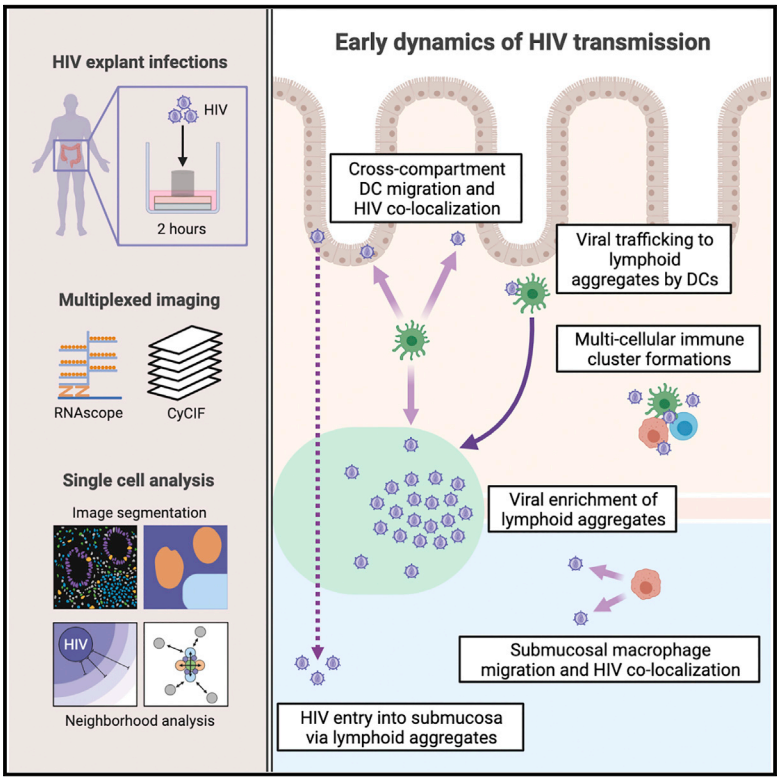

Authors

Heeva Baharlou, Nicolas Canete, Erica E. Vine, ..., Scott N. Byrne, Anthony L. Cunningham, Andrew N. Harman

Correspondence

heeva.baharlou@gmail.com (H.B.), andrew.harman@sydney.edu.au (A.N.H.)

In brief

Baharlou et al. develop an *in situ* analysis pipeline to map out initial human colorectal HIV transmission events, finding key target cells, tissue compartments, and cell:cell interactions underlying transmission. These results suggest hypotheses regarding mechanisms of HIV transmission and demonstrate the utility of pathogen transmission studies using intact human tissue.

Highlights

- *In situ* quantification pipeline of early host-pathogen interactions in human tissue
- Initial HIV enrichment in mucosal DCs and submucosal macrophages, but not $CD4^+$ T cells
- HIV preferentially localizes to lymphoid aggregates, mediating submucosal virus entry
- HIV rapidly alters cellular spatial organization to maximize uptake and infection

Baharlou et al., 2022, Cell Reports *40*, 111385
September 20, 2022
https://doi.org/10.1016/j.celrep.2022.111385

CellPress

Cell Reports

CellPress
OPEN ACCESS

Article

An *in situ* analysis pipeline for initial host-pathogen interactions reveals signatures of human colorectal HIV transmission

Heeva Baharlou,[1,2,*] Nicolas Canete,[1,2] Erica E. Vine,[1,2] Kevin Hu,[1,2] Di Yuan,[1,2] Kerrie J. Sandgren,[1,2] Kirstie M. Bertram,[1,2] Najla Nasr,[1,2] Jake W. Rhodes,[1,2] Martijn P. Gosselink,[1,3] Angelina Di Re,[1,3] Faizur Reza,[1,3] Grahame Ctercteko,[1,3] Nimalan Pathma-Nathan,[1,3] Geoff Collins,[1,3] James Toh,[1,3] Ellis Patrick,[1,4] Muzlifah A. Haniffa,[5,6,7] Jacob D. Estes,[8,9] Scott N. Byrne,[1,2] Anthony L. Cunningham,[1,2] and Andrew N. Harman[1,2,10,*]

[1]Centre for Virus Research, The Westmead Institute for Medical Research, 176 Hawkesbury Road, Westmead, NSW 2145, Australia
[2]The University of Sydney, School of Medical Sciences, Faculty of Medicine and Health Sydney, Sydney, NSW, Australia
[3]Department of Colorectal Surgery, Westmead Hospital, Westmead, NSW 2145, Australia
[4]The University of Sydney, School of Maths and Statistics, Faculty of Science, Sydney, NSW, Australia
[5]Biosciences Institute, The University of Newcastle, Newcastle upon Tyne, UK
[6]Wellcome Sanger Institute, Hinxton, UK
[7]Department of Dermatology and NIHR Newcastle Biomedical Research Centre, Newcastle Hospitals NHS Foundation Trust, Newcastle upon Tyne, UK
[8]Vaccine & Gene Therapy Institute, Oregon Health & Science University, Portland, OR, USA
[9]Division of Pathobiology & Immunology, Oregon National Primate Research Center, Oregon Health & Science University, Portland, OR, USA
[10]Lead contact
*Correspondence: heeva.baharlou@gmail.com (H.B.), andrew.harman@sydney.edu.au (A.N.H.)
https://doi.org/10.1016/j.celrep.2022.111385

SUMMARY

The initial immune response to HIV determines transmission. However, due to technical limitations we still do not have a comparative map of early mucosal transmission events. By combining RNAscope, cyclic immunofluorescence, and image analysis tools, we quantify HIV transmission signatures in intact human colorectal explants within 2 h of topical exposure. We map HIV enrichment to mucosal dendritic cells (DCs) and submucosal macrophages, but not $CD4^+$ T cells, the primary targets of downstream infection. HIV^+ DCs accumulate near and within lymphoid aggregates, which act as early sanctuaries of high viral titers while facilitating HIV passage to the submucosa. Finally, HIV entry induces recruitment and clustering of target cells, facilitating DC- and macrophage-mediated HIV transfer and enhanced infection of $CD4^+$ T cells. These data demonstrate a rapid response to HIV structured to maximize the likelihood of mucosal infection and provide a framework for *in situ* studies of host-pathogen interactions and immune-mediated pathologies.

INTRODUCTION

Thirty-seven million people are infected with HIV and, despite the introduction of pre-exposure prophylaxis, there were still 1.5 million new infections in 2020. Blocking transmission of HIV therefore remains a high global priority that requires an effective vaccine and, in the meantime, better prophylactic interventions. To achieve these goals, we need a better understanding of the initial events that govern transmission of HIV, particularly early viral interactions with antigen-presenting cells, such as dendritic cells (DCs) and macrophages, and their subsequent delivery of the virus to $CD4^+$ T cells (Vine et al., 2022).

Simian immunodeficiency virus challenge studies have shown that productive mucosal infection at the site of transmission precedes the detection of plasma viremia, and that the viral reservoir is rapidly seeded at this site within days of exposure (Deleage et al., 2019; Whitney et al., 2014). Concordant data have also been described in human studies (Chun et al., 1998; Colby et al., 2018). Due to technological limitations, early transmission studies have been limited to time points after initial viral integration/replication (Maric et al., 2021; Stieh et al., 2016; Vine et al., 2022) or the use of model systems, with human tissue studies mostly performed on isolated cells or by imaging of limited parameters (Bertram et al., 2019a; Ganor et al., 2010; Hladik et al., 2007; Rhodes et al., 2021; Trifonova et al., 2018; Vine et al., 2022). Thus, we still do not know the initial events that lead to mucosal HIV infection in the human tissues where transmission occurs.

The next stage in advancing our understanding of these events requires an *in situ* quantitative multi-parameter study to understand the relative involvement of multiple target cells within anatomically distinct tissue compartments. This "top down" approach is critical for establishing physiological relevance and guiding the rational selection of specific biological mechanisms for in-depth characterization studies. To our knowledge, no study has examined all these processes at once in the context of pathogen invasion of human tissue. Such studies have been hampered

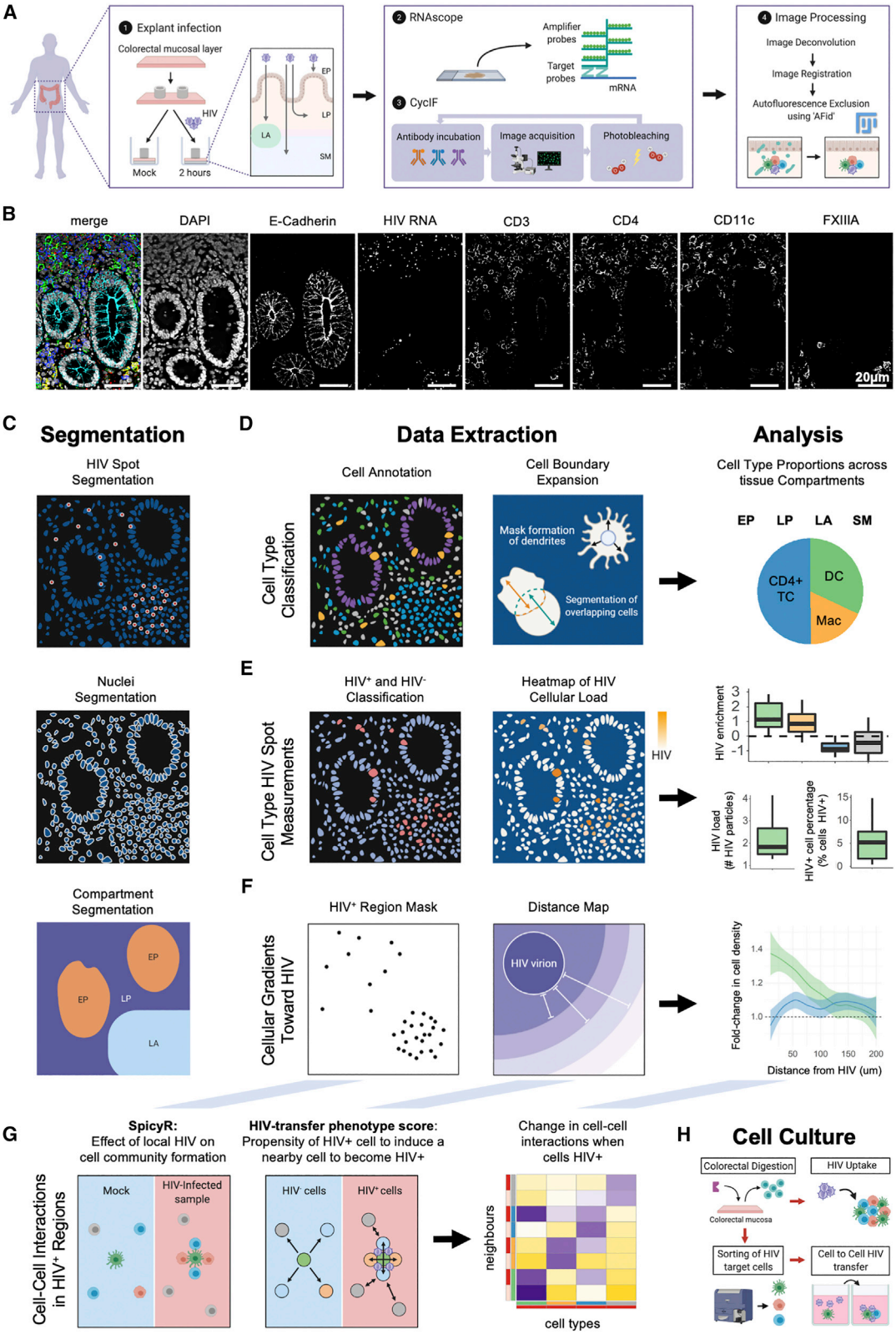

(legend on next page)

to date by a plethora of issues including parameter limitations of conventional microscopy, a lack of suitable image processing and analysis algorithms and, in the context of HIV, difficulties with *in situ* pathogen detection at early time points (Deleage et al., 2016).

We have recently pioneered the use of RNAscope to visualize clinically relevant HIV virions interacting with anogenital target cells *in situ* within 2 h of topical exposure (Bertram et al., 2019a; Rhodes et al., 2021). We have also designed post image acquisition algorithms to remove autofluorescence (Baharlou et al., 2020) and quantify cell interaction changes between disease states (Canete et al., 2022). In this study we have utilized these approaches as well as designed tools to segment full cell bodies more accurately, allowing us to quantify the signatures of HIV transmission across human colorectal tissue within 2 h of exposure. We have defined the spatial distribution of the three key colorectal HIV target cells (DCs, macrophages, and $CD4^+$ T cells) across all colorectal tissue compartments (epithelium [EP], lamina propria [LP], lymphoid aggregates [LAs], and submucosa [SM]) and shown how they respond to HIV. We show conclusively that HIV is initially enriched within mucosal (EP, LP, LA) DCs and submucosal macrophages, but not $CD4^+$ T cells and that the virus is preferentially enriched in LAs. We also provide strong circumstantial evidence that LP DCs traffic virus to LAs and that these structures themselves may provide a conduit for rapid HIV entry into the deeper submucosal layer, where it preferentially associates with macrophages. Finally, we show that HIV mucosal entry induces its target cells to form multi-cellular clusters within which HIV^+ DCs and macrophages preferentially cluster with $CD4^+$ T cells, leading to viral transfer and enhanced infection of $CD4^+$ T cells, supported by *ex vivo* data.

RESULTS

Analysis pipeline for mapping HIV-target cell interactions *in situ*

This study explores the interactions of HIV with its three key target cells—DCs, macrophages, and $CD4^+$ T cells—in human colorectal tissue at the very earliest time points following HIV challenge using a combination of RNAscope, multiplexed fluorescence microscopy, and a custom image-processing and analysis pipeline (Figure 1). Lab-adapted and transmitted/founder strains of HIV were applied to the apical surface of intact fresh human colorectal tissue for 2 h. RNAscope was performed to detect HIV RNA (virions), followed by cyclic immunofluorescence (CyCIF) microscopy, which was used to identify nuclei (DAPI), EP (E-Cadherin), $CD4^+$ T cells ($CD3^+CD4^+$), $CD4^-$ T cells ($CD3^+CD4^-$), DCs ($CD11c^+$), and macrophages ($FXIIIa^+$) (Figures 1A and 1B). While having little to no capacity for HIV uptake themselves, $CD4^-$ T cells (primarily $CD8^+$ T cells) served as a useful control for non-specific HIV-cell interactions *in situ*. We removed autofluorescence signal, a known feature of colorectal tissue imaging (Wizenty et al., 2018) post-acquisition using our autofluorescence identifier (AFid) algorithm (Baharlou et al., 2020) (Figures 1A and S1A). We next performed segmentation of HIV virions, cells, and tissue compartments (EP, LP, LA, SM) (Figure 1C). Cells were classified and segmented using a custom approach that estimates full cell bodies and allows two cells to physically overlap. This enabled virions to be accurately assigned to amorphous cells such as macrophages and DCs (Figures S1B and S1C). This pipeline allowed us to make compartment-specific measurements of target cell composition (Figure 1D), HIV status (HIV^+ versus HIV^-), virion load per cell (Figure 1E), target cell migration to/from HIV (Figure 1F), and the effect of HIV on interactions between target cells (Figure 1G).

To complement and validate these *in situ* data we used an orthogonal approach of flow cytometry analysis of HIV target cells following their dissociation from tissue and infection with HIV (Figures S1D–S1F). Using our HIV p24 uptake assay, we compared HIV uptake *in situ* with that of *ex-vivo*-dissociated cells. In addition, HIV-induced cell:cell interactions observed *in situ* (Figure 1G) were further investigated by sorting and infecting co-cultures of these cells to determine whether their interaction lead to enhanced viral transfer and infection (Figure 1H). Together these approaches enabled us to create an *in situ* quantitative map of how HIV is distributed across colorectal target cells and tissue compartments, as well as the HIV-induced cell:cell interactions that occur in the mucosa within 2 h post-exposure and prior to systemic viral spread.

HIV-target cell composition and distribution within human colorectal tissue

Using our analysis pipeline, we defined the relative proportion and density of HIV target cells within EP, LP, LAs, and SM in fresh

Figure 1. Analysis pipeline for mapping HIV-target cell interactions *in situ*

Custom image analysis pipeline to measure HIV-cell interactions in fresh human colorectal explant tissue exposed to HIV_{Bal} or HIV_{Z3678M} for 2 h and probed with RNAscope and CyCIF.

(A) Explant infection (1), staining with RNAscope (2), and CyCIF (3), and image processing protocol with autofluorescence removed digitally using "AFid" software (4).

(B) Representative images from staining in (A).

(C) Segmentation of virions, cell nuclei, and tissue compartments.

(D) Segmented nuclei were annotated (left) and expanded to estimate full cell bodies using a custom approach (center) (details in Figure S1C). Cell composition can then be determined across tissue compartments (right).

(E) Annotation of cells as HIV^+ ($\geq$1 virion) or HIV^- (left) and measurement of total HIV load per cell (center). This allowed for comparisons of HIV association with different target cells (right).

(F) Distance maps emanating from HIV particles (left and center) to measure changes in nearby cell density to infer potential cell migration to/from HIV.

(G) SpicyR determines if the local presence of HIV alters cell communities (left), while the "HIV-transfer phenotype score" measures the propensity of an HIV^+ cell to induce a nearby cell to become HIV^+ (center). Frequency of interactions can be visualized using a heatmap (right).

(H) Colorectal cell extraction and *ex vivo* HIV exposure to (1) compare 2 h HIV uptake with *in situ* results and (2) measure infection (intracellular p24 at 72 h) of $CD4^+$ T cells co-cultured with cells that exhibited HIV-induced interactions with $CD4^+$ T cells *in situ* in (G).

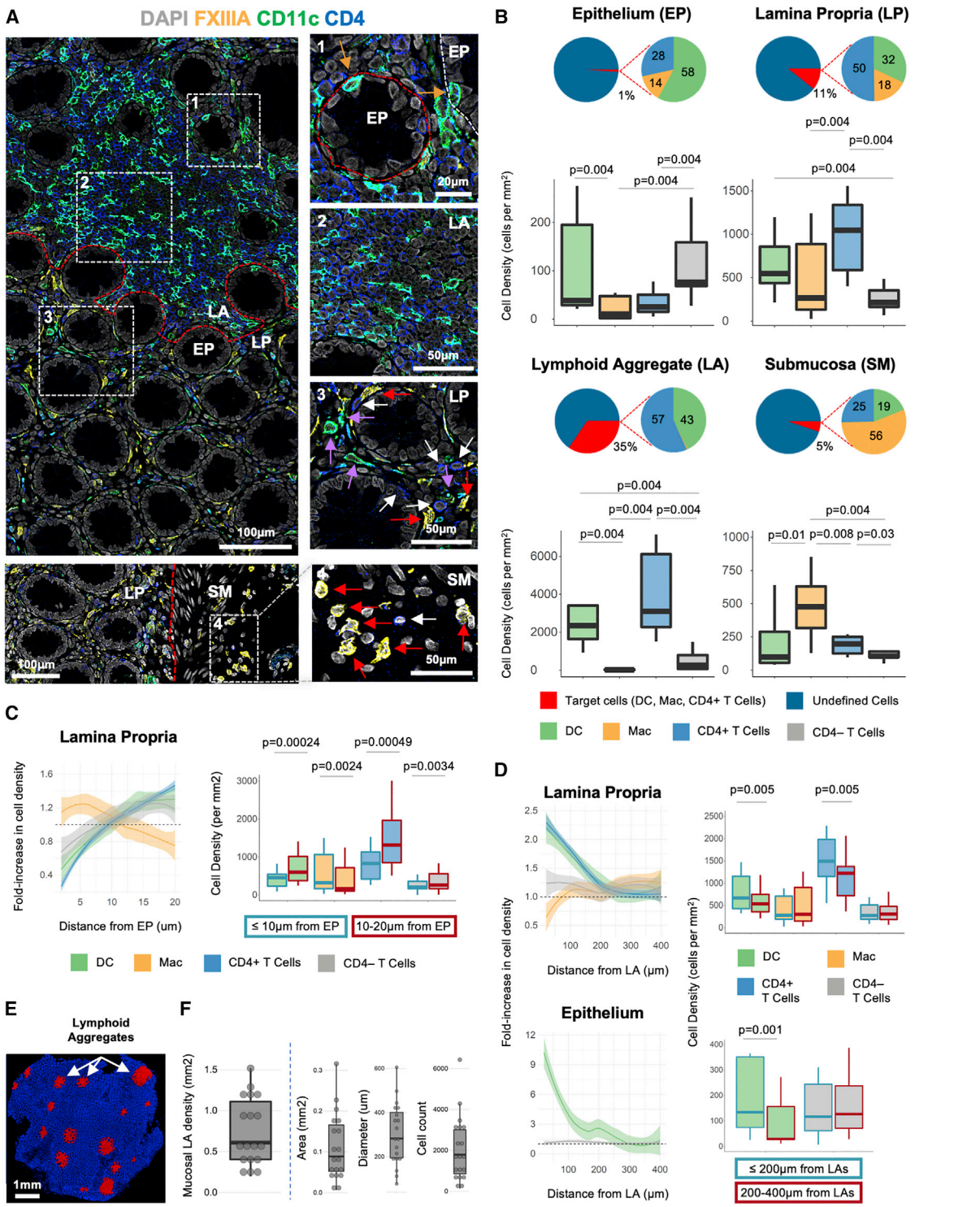

Figure 2. Distribution of HIV target cells across human colorectal tissue compartments

(A) Representative images of HIV target cells and their distribution. (1) DCs in the EP (brown arrows) near the LA. (2) LA DCs and CD4$^+$ T cells. (3) LP DCs (purple arrows), macrophages (red arrows), and CD4$^+$ T cells (white arrows). (4) Submucosal macrophages (red arrows). Broken red line, compartment borders.

(B) HIV target cell percentage among all cells, composition, and density across tissue compartments. CD4$^-$ T cells also shown.

(C) Change in LP target cell density with distance from EP. Left: fold change in target cell density (versus whole LP average) in 2 μm intervals from EP. Right: density of subsets in LP < 10 μm (blue border) or 10–20 μm (red border) from EP.

(legend continued on next page)

uninfected human colorectal tissue (Figures 2A and 2B). Although only 1% of EP cells were HIV target cells, DCs were the most abundant (58%), followed by $CD4^+$ T cells (28%) then macrophages (14%). Of the LP cells, 11% were HIV target cells, with $CD4^+$ T cells being most abundant (50%) followed by DCs (32%) and then macrophages (18%). In LAs, 35% of cells were HIV target cells consisting of $CD4^+$ T cells (57%) and DCs (43%) with negligible presence of macrophages. Five percent of SM cells were HIV target cells, with macrophages being most abundant (56%) followed by $CD4^+$ T cells (25%) and DCs (19%). Cell density measurements closely followed these trends for each tissue compartment. Thus, LAs and LP had the highest density of HIV target cells, with DCs and $CD4^+$ T cells dominating the mucosal layers and macrophages dominating the submucosal layer.

We next examined the spatial distribution of HIV target cells within each compartment. This was achieved by using the border between tissue compartments as an anchor and measuring changes in cell density from this reference point. LP macrophages were enriched <10 μm from the EP, while DCs, $CD4^+$ T cells, and $CD4^-$ T cells preferentially localized >10 μm away from the EP (Wilcoxon, $p < 0.005$ for all, Figure 2C). In LP, DCs, and $CD4^+$ T cells were enriched <200 μm from LAs (Wilcoxon, $p = 0.005$). This was also true for EP DCs (Wilcoxon, $p = 0.001$) but was not measurable for EP $CD4^+$ T cells due to their low frequency in EP (Figure 2D).

We next focused our attention on characterizing LAs as they contained the highest density of HIV target cells, particularly DCs and $CD4^+$ T cells (Figures 2A and 2B). LAs were present at a median density of 0.6 structures per mm^2 of tissue and varied in their area (median 0.09 mm^2; range 0.05–0.17 mm^2), diameter (median 283 μm; range 195–401 μm), and cell number (median 1,800 cells; range 860–3,015) (Figures 2E and 2F).

HIV viral particles are enriched in colorectal DCs and macrophages within 2 hours

We next assessed the interactions between HIV and its target cells using lab-adapted (BaL) or transmitted/founder (Z3678M) HIV strains. To ensure RNAscope probes were specific to HIV RNA we stained uninfected tissue and confirmed that no signal was detectable (Figure S2A). As our pipeline incorporates automated virion detection, we compared mock and HIV-treated explants to calculate the false detection rate. One particle per 1,000 cells was detected in mock versus 30 particles per 1,000 cells in HIV-treated explants, indicating that only 3% of HIV^+ cells in our treated samples were false positives (Figure S2B). To determine whether HIV was enriched among its target cells we measured the percentage of total HIV particles in this population (HIV percentage), as well as the percentage of all cells that were target cells (target cell percentage). A chi-square test was then performed to test for whether enrichment among target cells was significant. The formula "log2(HIV percentage/target cell percentage)" measured the relative level of HIV enrichment between images. Although the percentage of total HIV particles localizing to target cells varied across images, the majority showed significant HIV enrichment in target cells compared with the remaining undefined "other cells" (chi-square test, $p < 0.05$, Figure 3A), with up to 4-fold enrichment observed in some images (Figure 3A, bottom). Visual inspection confirmed the specificity of HIV association with target cells over other cells for HIV_{BaL} (Figure 3B) and HIV_{Z3678M} (Figure S2C). Using a similar approach, we tested for HIV enrichment in different target cell subsets and compared the degree of enrichment between populations (Figure 3C). As both HIV_{BaL} and HIV_{Z3678M} had similar trends in the degree of enrichment for each cell type (Figure S2D), we combined these data to increase statistical power. HIV was enriched among DCs and macrophages (Wilcoxon, $p < 0.01$), with higher enrichment (though not significant) in DCs (Figure 3C). Although, HIV associated with $CD4^+$ T cells, this occurred less than expected relative to their abundance (Wilcoxon, $p < 0.01$). In addition, $CD4^-$ T cells associated with HIV at the same frequency as their relative abundance, which is expected as they do not express HIV-binding receptors. We next analyzed HIV load in individual cells in each population to determine the differential amount of virus associated with each type of target cell. Combining RNAscope, spot segmentation (Figure 1C), and cell segmentation with cell body estimation (Figures S1B and S1C) enabled us to accurately measure single-particle differences between cells (Figure 3D). We pooled cells across all samples, stratified them by HIV particle count and measured the target cell composition within each group (Figure 3E). Among the 12,822 target cells analyzed, the majority (87%) contained only 1–3 HIV particles. Despite being the most prevalent cell type, $CD4^+$ T cells were under-represented in all groups, particularly those with higher HIV particle numbers. Indeed, the only HIV target cells we could detect with >8 virions were DCs and macrophages, but never $CD4^+$ T cells. This partly explains their relative HIV enrichment compared with $CD4^+$ T cells.

Finally, we sought to verify whether data derived by infection of intact explants with *in situ* analysis would mirror results from infecting *ex vivo* cells extracted from tissue and analyzed by flow cytometry (Figure 3F). This is important, as the study of HIV transmission in human tissue has been largely confined to studies on *ex vivo* isolated cells (Ahmed et al., 2015; Bertram et al., 2019b; Botting et al., 2017; Rhodes et al., 2019). Both approaches confirmed that the "percentage of cells containing HIV" and the "mean number of HIV particles per cell" were significantly greater for DCs and macrophages compared with $CD4^+$ T cells (Wilcoxon, $p < 0.01$). However, measurements on *ex vivo* cells showed the $CD4^+$ T cell "percentage" and "average" HIV measurements were significantly higher than $CD4^-$ T cells. In contrast no differences were observed *in situ*. This indicates that, at early time points *in situ*, HIV interactions with $CD4^+$ T cells are not yet measurably

(D) Change in EP or LP target cell density with distance from LAs. Left: fold change in density (versus whole EP or LP average) in 20 μm intervals from LAs. Right: density in EP or LP < 200 μm (blue border) or 200–400 μm (red border) from LAs.
(E) Representative image of LA distribution in colorectum. Image is segmentation mask of LA (red) and non-LA (blue) cells.
(F) Mucosal (EP + LP + LA) LA density (mm^2), average area (mm^2), diameter (μm), and cell count. n = 18 donors.
Density = cells per mm^2 of DAPI. Statistics: Wilcoxon signed-rank test. n = 12 donors for (A–E). LOESS curve of best fit for (C and D).

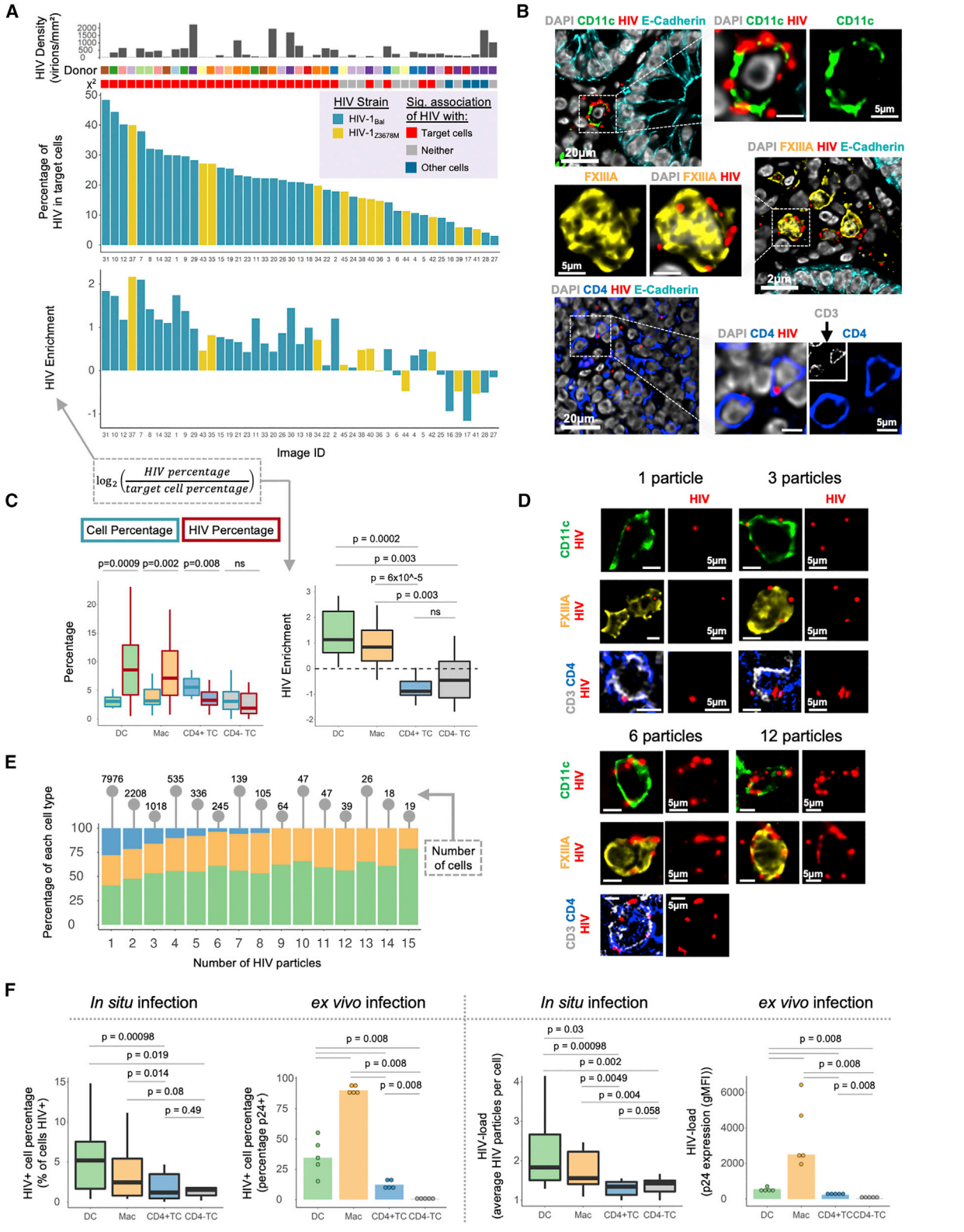

Figure 3. Assessment of interactions of HIV with colorectal target cells

(A) Target cell (DC, macrophage, CD4$^+$ T cells) association with HIV across all images in this study. Middle: percentage of image HIV particles associated with target cells. Bottom: HIV enrichment in target cells (log2(HIV percentage/target cell percentage)). Top: whole image HIV particle density (per mm^2 of DAPI), donor

(legend continued on next page)

different to that of a random interaction between HIV and a cell type with no HIV-binding capacity. Furthermore, *ex vivo* infection erroneously over-estimated macrophages as the dominant initial HIV-binding cell type, whereas *in situ* measurements showed DCs have a significantly higher mean HIV count per cell and a trend of higher HIV$^+$ cell frequency. These results highlight the importance of physiologically relevant quantitative *in situ* studies.

Taken together, these results demonstrate that HIV can enter human colorectal explants as early as 2 h after inoculation resulting in preferential association with DCs and macrophages, compared with CD4$^+$ T cells. Moreover, DCs and macrophages are capable of sampling larger quantities of virus at these early time points than other cells.

HIV localization patterns across colorectal tissue compartments and their associated target cells

We next turned our attention to tissue compartment-specific differences in the distribution of HIV particles and HIV-containing target cells. LAs contained the highest density of HIV particles reaching over 10,000 virions/mm^2 in several donors (Wilcoxon, $p < 3 \times 10^{-4}$, Figures 4A and S3A). HIV density was lowest in the EP and SM with the density in LP higher than EP (Wilcoxon, $p < 0.03$). To determine whether, upon EP penetration, HIV preferentially localizes to LP or LAs, we performed HIV enrichment analysis on compartments rather than cell types. We selected only LP and LA regions of images and compared the percentage of HIV in LAs with the expected percentage, defined as the percentage of the LP$^+$ LA area comprised of LAs (Figure 4B). Accordingly, values above or below expected (dotted line) indicate preferential localization to LAs or LP, respectively. Analyzing the residuals (distance of points from dotted line) revealed preferential localization to LAs over LP (Wilcoxon, $p = 0.0007$, Figure 4C), which was observable upon visual inspection of images (Figure 4D).

Having observed HIV enrichment in DCs and macrophages (Figure 3C), we next determined the compartments in which this enrichment occurred. In EP, LP, and LAs HIV preferentially localized to DCs, whereas in SM the virus preferentially localized to macrophages (Figure 4E). Representative images are shown in Figure 3B (top panel) for LP and Figure 4F for all other compartments. In LAs 25% of donors showed >50% of HIV localized to DCs, which is far more than other compartments (Figure 4E). Correspondingly, LA CD4+ T cells harbored significantly less HIV than expected based on their frequency. Therefore, LA DCs may be more primed for antigen uptake, which would partly explain the high levels of HIV observed in these cells in this compartment.

Comparing the degree of HIV enrichment in cells between compartments, we observed that EP DCs had a 2-fold HIV enrichment compared with LP and LA DCs. In contrast, SM macrophages had a median 4-fold enrichment compared with their LP counterparts (Wilcoxon, $p < 0.05$, Figure S3B). These compartment-specific differences in enrichment are explained by differences in cellular HIV load and the percentage of the population interacting with HIV. In particular, EP DCs had a higher HIV load per cell and a higher frequency of interactions with HIV, whereas SM macrophages had an increased frequency of HIV interactions, but a similar viral load to their LP counterparts (Wilcoxon, $p < 0.05$, Figures S3C and S3D).

Beyond mapping HIV-target cell interactions to compartments we also explored how HIV$^+$ cells were spatially distributed within compartments. Beginning with LP, we observed that, like uninfected tissue (Figure 2D), HIV$^+$ DCs and CD4$^+$ T cells were enriched near LAs (Figure S3E). However, this enrichment was greater for HIV$^+$ DCs and CD4$^+$ T cells than their HIV$-$ counterparts (paired two-sample t test, $p < 0.05$, Figure 4G), despite no difference in the frequency of viral particles between LA-proximal or -distal regions of the LP (Figure S3F). Interestingly, despite our previous observation of enrichment of LP macrophages near EP and also EP DCs near LAs (Figures 2C and 2D), we did not observe any enrichment of HIV$^+$ populations of these cells near these structures (data not shown).

In LAs themselves we measured HIV particle distribution using the formula for even-area concentric rings to divide these structures into roughly equal-area intervals (Figure S3G). Using this approach, we observed a significant increase in HIV density toward the center of LAs (Figure S3H). Stratifying LAs by size (Figure S3I), HIV particles could even be detected toward the center of larger LAs (>500 μm in diameter), suggesting there may be a mechanism to focus virus centrally within these structures (Figure S3J). Measuring HIV$^+$ cells rather than individual particles, we observed that DCs were the only HIV-containing cell type to increase significantly in frequency toward the center of LAs (Figures 4H and S3K). This suggests that DC-mediated transport may in part contribute to the central focusing of HIV within LAs.

Finally, as we were surprised that HIV interacted with macrophages in the deep SM layer as early as 2 h, we turned our attention to this compartment. We confirmed that HIV entry into the SM correlated with entry into the overlying mucosal layer (Pearson's $r = 0.62$, $p = 10^{-5}$, Figure S3L). Fitting a linear model of HIV

number (color-coded) and chi-square test (χ^2) of association indicating HIV enrichment in target cells (red), other cells (blue), or neither (gray); $p < 0.05$. HIV strain: blue bars, HIV_{Bal}; yellow bars, HIV_{Z3678M}.

(B) Representative images of colorectal target cells interacting with HIV_{Bal} particles.

(C) Left: cell type percentage (of all cells) versus percentage of all virions in cell type. Right: HIV enrichment as in (A). Statistics: Wilcoxon signed-rank test. n = 15 explants (images average).

(D) Representative images of target cells interacting with 1, 3, 6, or 12 HIV particles.

(E) HIV$^+$ target cells from all images were pooled and grouped by HIV load (1–15 particles). Composition of each cell type in each group is shown. Total cells in each group are annotated.

(F) HIV uptake after 2 h HIV_{Bal} treatment of explants with analysis by microscopy (*in situ* infection) or *ex vivo* isolated cells analyzed by flow cytometry (*ex vivo* infection). Percentage of cells interacting with HIV ($\geq$1 virion or p24+) (left) or HIV load per cell (virion number or p24 gMFI) (right) is shown. *In situ* infection: n = 11 donors, Wilcoxon rank-sign test; *ex vivo* infection: n = 5 donors, Wilcoxon rank-sum test.

n = 45 images from 15 explants (11 HIV_{Bal}, 4 HIV_{Z3678M}) from 12 donors for (A–E).

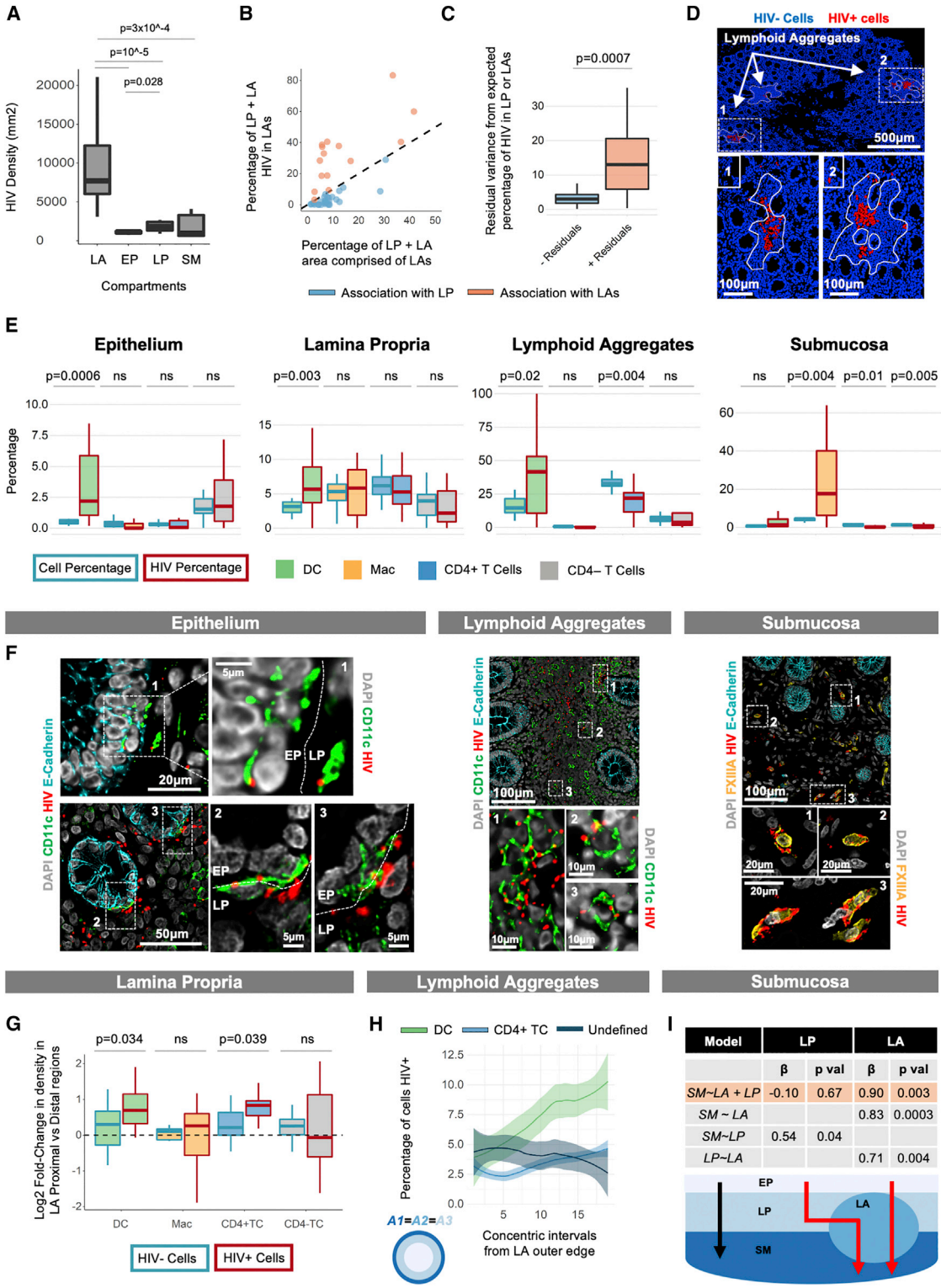

Figure 4. Differential HIV uptake across colorectal tissue compartments

(A) HIV density across tissue compartments. n = 10 images for each compartment (LA = 5, EP = 6, LP = 4, SM = 5 donors) (STAR Methods). Statistics: Wilcoxon rank-sum test.

(B) Percentage of virions in LAs versus percentage of image area (LP and LA only) comprised of LAs. Values above or below the line (y = x) indicate HIV enrichment in LAs or LP, respectively (STAR Methods). n = 44 images (16 donors).

(legend continued on next page)

density in the SM as a function of LA and LP HIV density, we found that only LAs significantly predicted SM HIV entry (β = 0.90, p = 0.003), suggesting LAs as the dominant route of HIV entry into the SM (Figure 3I; STAR Methods). Furthermore, we observed HIV particles throughout LAs, from the mucosal apical surface to the basal surface in the SM (Figure S3M), suggesting that viral trafficking through the length of LAs is possible. Finally, we present evidence to confirm that SM entry was not due to leakage of virus from the cloning cylinder during the culture period. First, we observed a high correlation between mucosal and SM HIV densities (Figure S3L), suggesting ordered entry of HIV into the SM from the mucosal layer. Second, HIV^+ macrophages were in both superficial (near crypt bases) and deeper regions of the SM (Figure S3N), whereas leakage would likely result in virus predominately in deeper regions, toward the bottom of the tissue. Finally, we collected the explant culture medium at the end of the culture period and confirmed that no HIV was present using a sensitive HIV detection assay (Figure S3O).

Together these results reveal substantial differences in HIV distribution across colorectal tissue compartments, with LAs as key initial entry sites appearing to facilitate HIV access to the SM. Furthermore, HIV enrichment in DCs and macrophages occurred only in the mucosa and SM, respectively. This highlights that it is not only the cell type, but also its compartmental residence, that determines the degree of interaction with HIV.

Colorectal DCs form gradients toward HIV within and across tissue compartments

We next explored potential mechanisms of differential HIV-target cell interactions by analyzing the spatial organization of target cells in relation to HIV. In particular, we measured changes in target cell density from HIV particles, where steadily increasing or decreasing density gradients were used to infer potential cell migration in response to HIV (Figure 1F). In EP, LP, and LAs we observed that DCs formed an increasing density gradient toward HIV, whereas T cells and macrophages did not (Figure 5A). The effect was most pronounced in LP to the extent that DCs were depleted in regions >300 μm from HIV. Similarly, SM macrophages formed an increasing density gradient toward HIV.

As DCs exhibited migratory patterns toward HIV in all three mucosal compartments, we investigated whether they showed patterns consistent with crossing tissue compartments in response to HIV. To this end, we measured whether LP DCs redistributed "toward" and "into" EP or LAs when these compartments contained HIV. Starting with EP, we classified EP cells into HIV^+ or HIV^- populations and measured the density of DCs in the LP $\leq$ 10 μm from each EP population. Compared with HIV^- EP, DCs were significantly more concentrated beneath (Figure 5B) and within HIV^+ EP (Figure 5C). Using a similar approach for LAs, we found that, compared with HIV^- LAs, LP DCs were significantly more enriched near HIV^+ LAs (Figure 5D) and DCs were present at a higher density within HIV^+ LAs (Figure 5E). In addition, DCs were more concentrated toward the outer edge of HIV^+ LAs, further supporting the idea that DCs may migrate into these structures in response to HIV (Figure 5F). We did not observe any difference in $CD4^+$ T cell density near or within HIV^+ versus HIV^- LAs.

Taken together, these results suggest that HIV enrichment in mucosal DCs and SM macrophages may relate to their ability to migrate toward incoming HIV, with DCs going as far as to cross tissue compartments in response to incoming virus.

HIV induces the formation of target cell clusters within which DCs and macrophages traffic virus to $CD4^+$ T cells

As cell:cell interactions are important for the spread of HIV (Bertram et al., 2019b; Bracq et al., 2018), we devised several spatial analysis tools to investigate the influence of HIV on interactions between target cells *in situ*.

We first used SpicyR (Canete et al., 2022), to compare cell:cell interactions between HIV^+ and HIV^- regions of treated explants to understand how HIV influences interactions, regardless of whether cells themselves are HIV^+. This analysis showed that, in HIV^+ regions, target cells cluster among each other in both LP and LAs. Interestingly, LP non-target $CD4^-$ T cells clustered among themselves in HIV^+ regions but not with HIV target cells (Figure 6A). In addition, there was no difference between HIV^- regions and the mock explants, confirming that clustering occurs specifically in response to HIV (Figure 6A). To verify that results are resistant to parameter variation, we ran SpicyR over a range of radius and distance cut offs (Figure S4A). Qualitative inspection of images confirmed the presence of clusters of DCs, macrophages, and $CD4^+$ T cells in HIV^+ regions (Figure 6B). Interestingly, clusters tended to form away from the EP in the central area between the crypts of Lieberkühn. We hypothesized that this was

(C) Positive and negative residuals (distance of points to line y = x) from (B), which represent the magnitude of HIV association with LA and LP, respectively. Statistics: Wilcoxon rank-sum test.
(D) Representative images showing preferential localization of HIV to LAs compared with the surrounding LP. Images are segmentation masks showing HIV^+ cells (red), HIV^- cells (blue), and outline of LAs.
(E) Cell type percentage (of all cells) versus percentage of all virions across target cells in tissue compartments. n = 15 explants from 12 donors (images averaged). Statistics: Wilcoxon signed-rank test.
(F) Representative images of DCs interacting with HIV in EP and LAs, and macrophage-HIV interactions in the SM. Broken line, EP-LP border.
(G) Log2 fold change in HIV^- or HIV^+ cell density in LA-proximal ($\leq$400 μm) versus -distal (400–800 μm) regions of LP. Paired regions only used if each contained at least 5 HIV^+ and 5 HIV^- cells. DC: 19 LAs (5 donors); Mac: 8 LAs (3 donors); $CD4^+$ TC: 15 LAs (6 donors); $CD4^-$ TC: 12 LAs (5 donors) Statistics: paired t test (normality assessed by Q-Q plot).
(H) Percentage of mucosal LA DCs, $CD4^+$ T cells, or undefined cells (not a DC, macrophage, or T cell) that are HIV^+ in intervals from the outer edge (x = 1) to center (x = 20) of HIV^+ LAs ($\geq$2 virions) (STAR Methods). n = 112 LAs (14 donors). Statistics: Figure S4K. LOESS curve of best fit.
(I) Linear models of compartment HIV density to assess whether SM HIV density ("*SM*") is dependent on LP ("*LP*") or LA HIV density ("*LA*"). β weights and p values shown. Schematic of model results showing LA to SM HIV entry (red line) as the most likely pathway. n = 14 donors.
Density = cells or virions per mm^2 of DAPI.

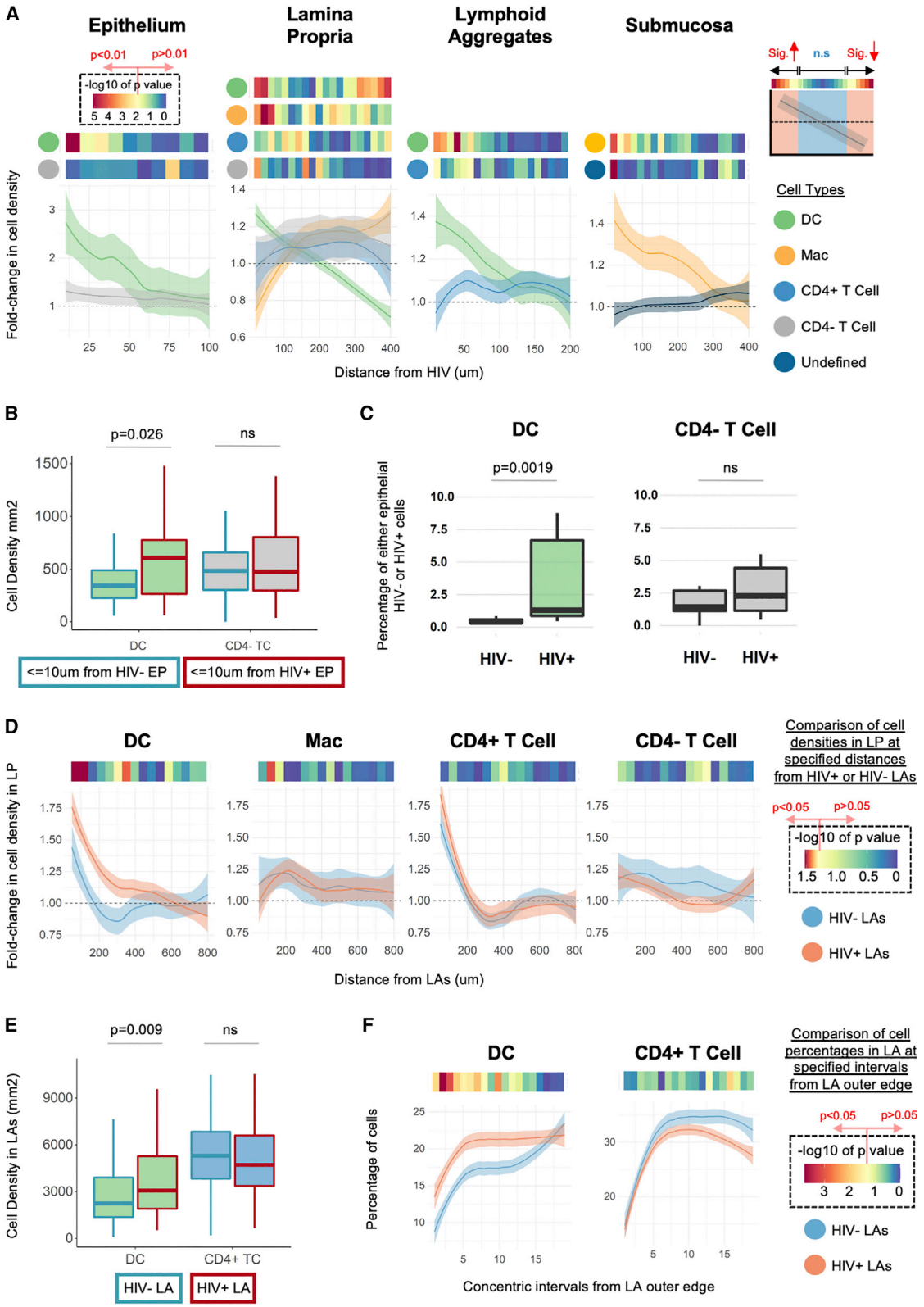

(legend on next page)

due to target cell migration away from the EP interface in response to incoming HIV. To investigate this, we devised a method of temporal inference to model the progression of HIV entry into the mucosa (STAR Methods). Here, images were divided into 100 μm^2 windows, each classified as "naive" (HIV density = 0), "early" (HIV density EP > LP), or "late" (HIV density EP < LP) in terms of HIV entry, with changes in target cell density measured close and far from the EP interface at each stage. Results showed that, like uninfected tissue, macrophages were enriched near the EP in naive regions; however, early in response to HIV they migrate deeper and persist there in the late phase (Figure S4B). Interestingly we found that $CD4^+$ T cells also migrate away from the EP, but only in the late phase, whereas $CD4^-$ T cells showed no change throughout the phases of entry. Curiously, DCs also showed no difference, although we can presume that this is due to their dual role of migration toward HIV^+ EP (Figures 5B and 5C) as well as forming part of the central clusters in the LP (Figures 6A and 6B). These results suggest that a secondary effect of colorectal HIV entry is the rapid formation of a target cell-enriched community slightly distal to the site of entry, thus creating an ideal environment for cell-to-cell viral transfer.

We next investigated potential cell to cell HIV transfer. As HIV is present at the interface between cells during active viral transfer (Garcia et al., 2005; McDonald et al., 2003; Wang et al., 2007, 2008; Yu et al., 2008), cells engaged in transfer would both appear HIV^+ in our dataset. Accordingly, we devised a "HIV-transfer phenotype score" to measure the change in association between cells when they both contain HIV. In brief, the frequency of HIV^+ cell interactions with either HIV^+ or HIV^- cells was calculated using neighborhood analysis (Schapiro et al., 2017) and the transfer score defined as the difference in HIV^+:HIV^+ and HIV^+:HIV^- interaction frequencies. This was used as a proxy for viral transfer (STAR Methods). Results showed that HIV^+ DCs in LP and LAs, and macrophages in LP, had the highest transfer scores to $CD4^+$ T cells (~50% increase in images showing significant interactions) (Figure 6C, dotted boxes). Interestingly, we also observed considerable transfer scores between HIV^+ DCs and macrophages. Importantly, transfer scores were close to 0 for $CD4^-$ T cells in LP, which are known to not transfer virus, as well as "unknown" cells in LAs. Potential transfer events were visually observable between DCs/macrophages and $CD4^+$ T cells (Figures 6D and S4C) or between DCs and macrophages themselves (Figure S4D) in both HIV_{BaL}- and HIV_{Z3678M}-treated explants. As transfer increases recipient cell HIV levels, we investigated whether $CD4^+$ T cell interactions with DCs/macrophages was associated with increased T cell HIV load. Measuring cell body overlap as a proxy for an active interaction (STAR Methods), we found that $CD4^+$ T cell viral load was significantly positively associated with interactions with DCs, but not macrophages (Figure 6E). Importantly, DCs did not interact with $CD4^-$ T cells regardless of their (incidental) association with HIV (Figure S4E), which confirms specificity and controls for the possibility of DC migration toward HIV (Figure 5A) driving the association. These results provide *in situ* quantitative evidence of cell-to-cell HIV transfer in intact tissue leading to increased $CD4^+$ T cell HIV levels within just 2 h of exposure.

Having observed HIV-induced clustering among target cells and potential viral transfer *in situ we* determined whether this led to increased viral replication in $CD4^+$ T cells *ex vivo*. We sorted all colorectal HIV target cells and co-cultured DCs or macrophages with autologous $CD4^+$ T cells prior to infection with a transmitted founder HIV strain and subsequent assessment of $CD4^+$ T cell infection 72 h later. We found that the presence of DCs or macrophages significantly enhanced infection of $CD4^+$ T cells (Figure 6F). To determine whether enhancement was mediated by viral transfer we next infected DCs and macrophages prior to the addition of activated PBMC-derived $CD4^+$ T cells. The results showed that both DCs and macrophages mediated HIV transfer to $CD4^+$ T cells leading to increased viral replication but that this effect was significantly greater for DCs (Figure 6G).

All together, these results suggest that mucosal HIV entry induces its target cells to cluster together forming a community in which DCs and macrophages deliver virus to $CD4^+$ T cells, facilitating infection of these cells within the mucosa itself.

DISCUSSION

In this study we developed a pipeline for multiplexed *in situ* quantification of initial host-pathogen transmission events and applied it to study human colorectal HIV transmission within 2 h of exposure. This was made possible by a combination of RNAScope, CyCIF, and image analysis algorithms to enable accurate quantification. In particular, RNAscope overcame issues of low signal-to-noise inherent in antibody- and fluorophore-tagged HIV detection approaches (Campbell et al., 2007; Deleage et al., 2016; Eugenin and Berman, 2016; Prevedel et al., 2019) and, when combined with CyCIF, enabled quantitative comparison of

Figure 5. Cellular gradients in response to HIV

(A) Fold change in cell density (versus compartment average) in 10 μm (EP) or 20 μm (LP, LA, SM) intervals from HIV. n = 45 images (12 donors). Statistics: Wilcoxon signed-rank test comparing interval cell-type density with the compartment average.

(B) LP DC and $CD4^-$ T cell density within 10 μm of HIV^+ EP (≥1 virions) or HIV^- EP (STAR Methods). n = 40 images (12 donors). Statistics: Wilcoxon signed-rank test.

(C) EP cells were classified as HIV^+ or HIV^- and the percentage of each population comprising DCs or $CD4^-$ T cells was measured. n = 33 images (11 donors). Statistics: Wilcoxon signed-rank test.

(D) Fold change in cell density (versus LP average) in 50 μm intervals from HIV^+ (≥2 virions) or HIV^- (<2 virions) LAs. n = 38 images (12 donors). Statistics: Wilcoxon signed-rank test comparing cell density between intra-image HIV^+ and HIV^- LAs for each interval.

(E) Density of DCs or $CD4^+$ T cells in mucosal HIV^+ versus HIV^- LAs. Statistics: Wilcoxon rank-sum test comparing cell density between HIV^- LAs (n = 84) and HIV^+ LAs (n = 82) in 11 donors.

(F) DC and $CD4^+$ T cell frequency (percentage of all cells) in intervals of mucosal HIV^+ versus HIV^- LAs in (E), from their outer edge (x = 1) toward their center (x = 20). Statistics: Wilcoxon rank-sum test comparing cell frequencies in each interval between HIV^+ and HIV^- LAs.

Density = cells per mm^2 of DAPI. LOESS curve of best fit for (A, D, and F). Heatmaps centered at p = 0.01 (A) or p = 0.05 (D and F).

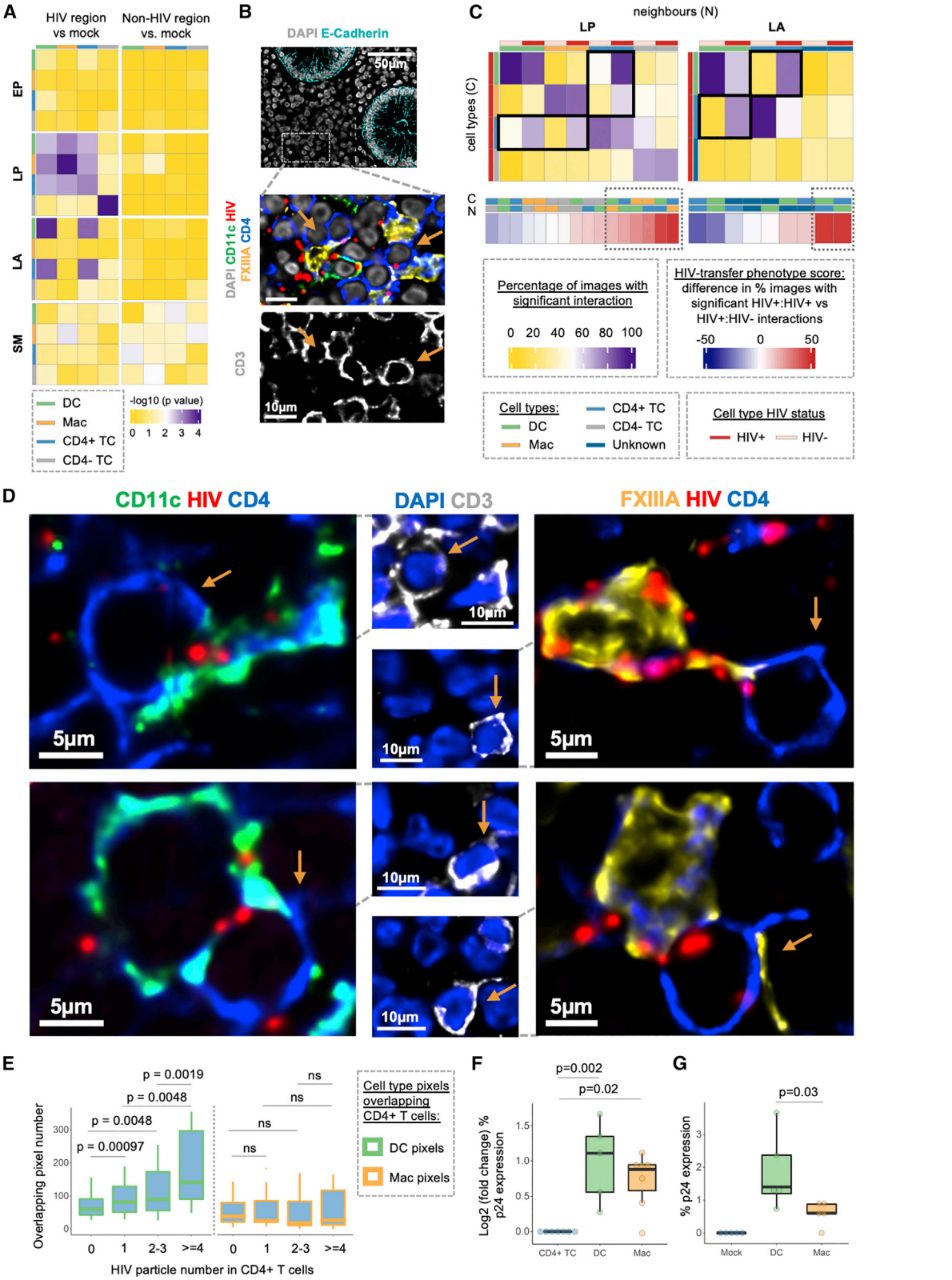

(legend on next page)

HIV localization to DCs, macrophages, $CD4^+$ T cells, and $CD4^-$ T cells (as a control) in four colorectal tissue compartments. Our AFid tool reduces false identification of HIV^+ cells due to autofluorescence (Baharlou et al., 2020). Our segmentation approach allows cell overlap to outline full cell bodies. This enables accurate assignment of HIV particles to amorphous cells, such as DCs and macrophages (Figure S1), while ensuring key cell:cell interactions are not missed as HIV can be transmitted between cells via membranous extensions (Eugenin et al., 2009; Nikolic et al., 2011). Finally, we employed spatial techniques to investigate cell:cell spread of HIV including our recently developed SpicyR algorithm (Canete et al., 2022), and a HIV-transfer phenotype score derived from neighborhood analysis (Schapiro et al., 2017). Together these approaches enabled us to dissect early transmission events *in situ* and provides a framework for *in situ* quantification of cellular microenvironment changes that could be applied to a range of disease and physiological settings.

The relative involvement of different HIV target cells in initial viral uptake is fundamental to understanding the determinants of transmission. However, this has not been previously described in intact primary human colorectal tissue. We reveal that HIV is preferentially enriched in DCs and macrophages rather than $CD4^+$ T cells, with DCs exhibiting the highest per-cell viral sampling capacity (Figure 3). Importantly, this was not replicable upon infection of *ex vivo* isolated rectal cells where macrophages were the dominant initial target cell, in agreement with previous work (Gurney et al., 2005). We postulate that this difference is because the tissue microenvironment is a critical factor in HIV target cell migration and viral interactions, as illustrated in this study and others (Cavarelli et al., 2013; Ganor et al., 2010; Imle et al., 2019; Zhou et al., 2018). This reinforces the importance of *in situ* studies to accurately define initial host-pathogen interactions.

A key strength of this study is the analysis of tissue compartments (Figures 4 and 5), which revealed that HIV enrichment in DCs and macrophages was specific to the mucosa and submucosa, respectively, and that HIV preferentially localizes to LAs. Mucosal DCs and submucosal macrophages steadily increased in density toward HIV particles, suggestive of migration to sites of HIV entry. LP DCs also appeared capable of crossing compartments to sample HIV, which has been observed for epithelium (Cavarelli et al., 2013), but which we report here for LAs. As such, migration may be a key mechanism of early viral enrichment in these populations. This may be the function of one or more subsets of either DCs or macrophages, as subset-specific differences in both migratory capacity (Domanska et al., 2022) and HIV binding (Bertram et al., 2019a; Rhodes et al., 2021) have been observed. HIV binding itself appeared to influence cell location with LP HIV^+ DCs and $CD4^+$ T cells tending to locate near LAs. This could represent specific cell subsets in LA-adjacent regions, which are known to vary in murine studies of Peyer's patches (Bonnardel et al., 2015) but are unstudied in humans. Another possibility, at least for DCs, is that HIV binding induces enhanced LA-directed migration and entry. This is supported by the increased DC density in HIV^+ versus HIV^- LAs and the preponderance of HIV^+ DCs in these structures. Compartment-based analysis also revealed that LAs are key HIV-containing compartments within 2 h of exposure to the virus. This may be due to delivery by HIV^+ DCs or other cells in the adjacent LP, or via follicle-associated epithelium and resident M cells, which is a key site of entry for other enteric pathogens (Kobayashi et al., 2019). As LAs are enriched in rectal tissue (Langman and Rowland, 1986), contain abundant HIV target cells and are known sites of HIV persistence (Chun et al., 2008), rapid access to these structures may facilitate sustained infection and early reservoir formation within the mucosa. Indeed, naive $CD4^+$ T cells are enriched in LAs (Fenton et al., 2020) and are amenable to both viral transfer and activation by HIV^+ DCs, which can promote latency (Cameron et al., 2010) and HIV-susceptible Th17 programs (Koh et al., 2020; Renault et al., 2022; Stieh et al., 2016). Entry into LAs but not LP was also associated with increased SM HIV levels, suggesting LAs as a possible conduit for HIV access to the underlying SM. This could be through direct passage as LAs traverse the muscularis mucosa barrier (Fenton et al., 2020) and HIV easily penetrates deep into LAs (Figures S3H–S3J). Alternatively, as HIV disseminates via lymphatics (Deleage et al., 2019), it may use the extensive LA lymphatic network (Fenton et al., 2020) to gain access to the SM, through which mucosal lymphatics drain (Unthank and Bohlen, 1988).

$CD4^+$ T cells are the major initial targets of HIV integration and productive infection (Gupta et al., 2002; Maric et al., 2021; Stieh et al., 2016). However, the early events leading to infection remain poorly understood. DCs and macrophages facilitate HIV transfer and enhanced $CD4^+$ T cell infection *in vitro*; however, *in situ* characterization using human tissue is lacking and mostly qualitative (Vine et al., 2022). Using our SpicyR algorithm and temporal inference we show that, after HIV penetrates the EP, HIV target cells appear to move away from the EP and form clusters consisting of DCs, macrophages, and $CD4^+$

Figure 6. Signatures of HIV-induced cell:cell interactions *in situ*

(A) SpicyR analysis of differential cell:cell localization in HIV^+ regions or HIV^- regions versus mock-treated images in the EP, LP, LA, or SM (STAR Methods). Purple indicates significant ($p < 0.01$) interactions. n = 45 images (12 donors).

(B) Representative image of HIV target cells clustering (brown arrows) in an HIV^+ region located away from the EP interface.

(C) "HIV-transfer phenotype score" to estimate viral transfer between cells (STAR Methods). Frequency of HIV^+ target cell (rows) interactions with HIV^- or HIV^+ neighbors (columns) in LP or LAs. Colors: percentage of images with significant ($p < 0.005$) interactions (yellow-purple) or the HIV-transfer phenotype score (blue-red gradient), which is the difference in frequency between HIV^+:HIV^+ and HIV^+:HIV^- interactions. Key interactions encased by boxes. n = 45 images (12 donors).

(D) Representative images of DCs and macrophages interacting with $CD4^+$ T cells (brown arrow) where HIV_{Bal} is present at the interface between cells.

(E) Number of DC (CD11c) or macrophage (FXIIIa) pixels overlapping with the body of $CD4^+$ T cells that harbor varying levels of HIV particles. n = 11 images (5 donors). Statistics: Wilcoxon rank-sum test.

(F) HIV co-culture assay. Primary colorectal $CD4^+$ T cell p24 expression 72 h after HIV_{Z3678M} treatment (2 h, MOI = 1) of either $CD4^+$ T cells alone (n = 7), or with added DCs (n = 5) or macrophages (n = 7) (10:1 ratio). Statistics: Wilcoxon rank-sum test comparing p24 fold change in co-cultures versus lone $CD4^+$ T cell infections.

(G) HIV transfer assay. PBMC-derived $CD4^+$ T cell p24 expression 72 h after HIV_{Z3678M} or mock (PBS) treatment (2 h, MOI = 1) of primary colorectal DCs or macrophages with subsequent addition of $CD4^+$ T cells. Statistics: Wilcoxon rank-sum test to compare.

T cells (Figure 6). This may occur temporally as our data suggest that macrophages migrate away from the EP initially, followed by $CD4^+$ T cells. Importantly, this was specific to HIV target cells and creates an ideal setting for viral transfer between cell types. Indeed, using a scoring system for potential HIV transfer events, we showed that, upon HIV binding, DCs and macrophages preferentially cluster with $CD4^+$ T cells, with virus present at the cellular interface. Interestingly, $CD4^+$ T cell HIV load was tightly correlated with their physical overlap with DCs, suggesting that the early presence of high viral loads in $CD4^+$ T cells may be dependent on their interactions with DCs. The lack of this association for macrophages may be due to lower levels of viral transfer, or a lack of physical overlap during interactions with T cells, unlike DCs which can entirely envelope $CD4^+$ T cells during transfer (Felts et al., 2010). Finally, we assessed infection of rectal tissue-derived co-cultures and confirmed viral transfer and enhanced infection of $CD4^+$ T cells by both DCs and macrophages, in agreement with other studies (Bertram et al., 2019a; Nasr et al., 2014; Rhodes et al., 2021). This provides the strongest evidence to date that viral transfer to $CD4^+$ T cells occurs as early as 2 h within the mucosa.

In summary, this study contributes quantitative *in situ* data on the initial events of HIV transmission in intact human mucosal explant tissue. Although some of the findings of this study are circumstantial, we believe they give rise to important hypotheses regarding HIV transmission. Particularly, the role of niche-specific cell subsets, the drivers of cell recruitment and cell:cell interactions at sites of HIV entry, and the possibility of LAs as key sites of early viral amplification, persistence, and extra-mucosal dissemination. We anticipate that recent advancements in high-parameter imaging modalities (Baharlou et al., 2019; Lewis et al., 2021), animal models and human organoid systems (Kim et al., 2020) will allow unprecedented insight regarding the early determinants of HIV transmission. The approach and results presented here provide a foundation for such future studies, which could inform prophylactic interventions or the design of a mucosal vaccine.

Limitations of the study

Cells were defined as HIV^+ if they spatially overlapped with HIV particles, meaning that some will be false positive due to random encounter. We worked around this limitation with comparative rather than absolute measurements such as HIV enrichment (HIV^+ cell frequency/cell frequency). Precise identification of virion-cell interactions would require a sensitive reporter construct that produces a signal following the virion-membrane binding event. However, this would be challenging as the virus rapidly contacts multiple cell types in tissue and so downstream virion-cell interactions would produce false negatives.

Increasing/decreasing cell density gradients were used to infer cell migration to and from areas of tissue. Formal proof would require real-time imaging of virions and cells in fresh human explant tissue, which is technically challenging if not impossible with current technologies.

The goal of our study was to map out the early host-cell interactions that characterize colorectal HIV transmission. However, our system is unable to determine the relative contribution of these early interactions to downstream mucosal infection. Future studies may address this by combining pro-longed explant culture, rapid targeted inhibition of cell subsets, and a reporter for downstream productive infection (Stieh et al., 2016). However, studying the role of newly migrated blood-derived immune cells in mucosal infection would likely require small animal models (Gillgrass et al., 2020).

STAR★METHODS

Detailed methods are provided in the online version of this paper and include the following:

- KEY RESOURCES TABLE
- RESOURCE AVAILABILITY
  - Lead contact
  - Materials
  - Data and code availability
- EXPERIMENTAL MODEL AND SUBJECT DETAILS
  - Human subjects
  - Cell lines
- METHOD DETAILS
  - HIV-1 virus production
  - Tissue digestion
  - HIV uptake assay
  - Target cell selection and sorting
  - HIV co-culture assay
  - HIV transfer assay
  - HIV assessment by flow cytometry
  - PBMC-derived CD4+ T cell isolation
  - HIV explant infection
  - Tissue embedding and sectioning
  - RNAScope
  - Cyclic immunofluorescence staining and image acquisition
  - Image acquisition
- QUANTIFICATION AND STATISTICAL ANALYSIS
  - Image deconvolution and registration
  - Autofluorescence removal
  - HIV spot segmentation
  - Cell segmentation and Classification
  - Tissue compartment segmentation
  - Data extraction in Matlab
  - Analysis in R
  - HIV enrichment and association testing in cells
  - HIV enrichment testing in tissue compartments
  - Measuring HIV density across tissue compartments
  - Cellular spatial distribution within compartments
  - Cellular gradients in response to HIV
  - Analysis of pathways for submucosal HIV entry
  - SpicyR analysis
  - Temporal inference analysis
  - HIV-transfer phenotype score
  - Association between T cell HIV-load and DC/macrophage interaction

SUPPLEMENTAL INFORMATION

Supplemental information can be found online at https://doi.org/10.1016/j.celrep.2022.111385.

ACKNOWLEDGMENTS

This work was funded by the National Health and Medical Research Council Ideas grant (GNT1181482). The authors would like to acknowledge the Westmead Cell Imaging and Flow Cytometry Core Facilities, supported by the Westmead Institute, Westmead Research Hub, Cancer Institute New South Wales.

AUTHOR CONTRIBUTIONS

Conceptualization, H.B. and A.N.H.; methodology, H.B., A.N.H., N.C., E.E.V., K.M.B., and J.W.R.; experimental investigation, H.B., E.E.V., and D.Y.; computational analysis, H.B., N.C., K.H., and E.P.; novel reagents and samples, J.T., G.C., N.P., G.C., F.R., A.D.R., and M.P.G,; visualization, H.B., K.H., and E.E.V.; writing, H.B. and A.N.H.; funding acquisition, A.N.H. and A.L.C. intellectual input and critical revisions, H.B., A.N.H., A.L.C., E.E.V., K.J.S., K.M.B., N.-P.N., S.N.B., J.D.E., and M.A.H. All authors read and approved of the manuscript.

DECLARATION OF INTERESTS

The authors declare no competing interests.

Received: April 18, 2022
Revised: July 7, 2022
Accepted: August 29, 2022
Published: September 20, 2022

REFERENCES

Ahmed, Z., Kawamura, T., Shimada, S., and Piguet, V. (2015). The role of human dendritic cells in HIV-1 infection. J. Invest. Dermatol. *135*, 1225–1233.

Baharlou, H., Canete, N.P., Cunningham, A.L., Harman, A.N., and Patrick, E. (2019). Mass cytometry imaging for the study of human diseases-applications and data analysis strategies. Front. Immunol. *10*, 2657.

Baharlou, H., Canete, N.P., Bertram, K.M., Sandgren, K.J., Cunningham, A.L., Harman, A.N., and Patrick, E. (2020). AFid: a tool for automated identification and exclusion of autofluorescent objects from microscopy images. Bioinformatics *37*, 559–567.

Baharlou, H., Canete, N.P., Vine, E.E., Hu, K., Yuan, D., Sandgren, K., Bertram, K., Nasr, N., Rhodes, J.W., Gosselink, M.P., et al. (2022). An in situ analysis pipeline for initial host-pathogen interactions reveals signatures of human colorectal HIV transmission. https://doi.org/10.5281/zenodo.6992156.

Baron, R.M., and Kenny, D.A. (1986). The moderator-mediator variable distinction in social psychological research: conceptual, strategic, and statistical considerations. J. Pers. Soc. Psychol. *51*, 1173–1182.

Battich, N., Stoeger, T., and Pelkmans, L. (2013). Image-based transcriptomics in thousands of single human cells at single-molecule resolution. Nat. Methods *10*, 1127–1133.

Bertram, K.M., Botting, R.A., Baharlou, H., Rhodes, J.W., Rana, H., Graham, J.D., Patrick, E., Fletcher, J., Plasto, T.M., Truong, N.R., et al. (2019a). Identification of HIV transmitting CD11c(+) human epidermal dendritic cells. Nat. Commun. *10*, 2759.

Bertram, K.M., Tong, O., Royle, C., Turville, S.G., Nasr, N., Cunningham, A.L., and Harman, A.N. (2019b). Manipulation of mononuclear phagocytes by HIV: implications for early transmission events. Front. Immunol. *10*, 2263.

Bonnardel, J., Da Silva, C., Henri, S., Tamoutounour, S., Chasson, L., Montanana-Sanchis, F., Gorvel, J.P., and Lelouard, H. (2015). Innate and adaptive immune functions of peyer's patch monocyte-derived cells. Cell Rep. *11*, 770–784.

Botting, R.A., Rana, H., Bertram, K.M., Rhodes, J.W., Baharlou, H., Nasr, N., Cunningham, A.L., and Harman, A.N. (2017). Langerhans cells and sexual transmission of HIV and HSV. Rev. Med. Virol. *27*.

Bracq, L., Xie, M., Benichou, S., and Bouchet, J. (2018). Mechanisms for cell-to-cell transmission of HIV-1. Front. Immunol. *9*, 260.

Cameron, P.U., Saleh, S., Sallmann, G., Solomon, A., Wightman, F., Evans, V.A., Boucher, G., Haddad, E.K., Sekaly, R.-P., Harman, A.N., et al. (2010). Establishment of HIV-1 latency in resting CD4(+) T cells depends on chemokine-induced changes in the actin cytoskeleton. Proc. Natl. Acad. Sci. USA *107*, 16934–16939.

Campbell, E.M., Perez, O., Melar, M., and Hope, T.J. (2007). Labeling HIV-1 virions with two fluorescent proteins allows identification of virions that have productively entered the target cell. Virology *360*, 286–293.

Canete, N.P., Iyengar, S.S., Ormerod, J.T., Baharlou, H., Harman, A.N., and Patrick, E. (2022). spicyR: spatial Analysis of in situ cytometry data in R. Bioinformatics *38*, 3099–3105.

Carpenter, A.E., Jones, T.R., Lamprecht, M.R., Clarke, C., Kang, I.H., Friman, O., Guertin, D.A., Chang, J.H., Lindquist, R.A., Moffat, J., et al. (2006). CellProfiler: image analysis software for identifying and quantifying cell phenotypes. Genome Biol. *7*, R100.

Cavarelli, M., Foglieni, C., Rescigno, M., and Scarlatti, G. (2013). R5 HIV-1 envelope attracts dendritic cells to cross the human intestinal epithelium and sample luminal virions via engagement of the CCR5. EMBO Mol. Med. *5*, 776–794.

Chun, T.W., Engel, D., Berrey, M.M., Shea, T., Corey, L., and Fauci, A.S. (1998). Early establishment of a pool of latently infected, resting CD4(+) T cells during primary HIV-1 infection. Proc. Natl. Acad. Sci. USA *95*, 8869–8873.

Chun, T.W., Nickle, D.C., Justement, J.S., Meyers, J.H., Roby, G., Hallahan, C.W., Kottilil, S., Moir, S., Mican, J.M., Mullins, J.I., et al. (2008). Persistence of HIV in gut-associated lymphoid tissue despite long-term antiretroviral therapy. J. Infect. Dis. *197*, 714–720.

Colby, D.J., Trautmann, L., Pinyakorn, S., Leyre, L., Pagliuzza, A., Kroon, E., Rolland, M., Takata, H., Buranapraditkun, S., Intasan, J., et al. (2018). Rapid HIV RNA rebound after antiretroviral treatment interruption in persons durably suppressed in Fiebig I acute HIV infection. Nat. Med. *24*, 923–926.

Damond, N., Engler, S., Zanotelli, V.R.T., Schapiro, D., Wasserfall, C.H., Kusmartseva, I., Nick, H.S., Thorel, F., Herrera, P.L., Atkinson, M.A., et al. (2019). A map of human type 1 diabetes progression by imaging mass cytometry. Cell Metabol. *29*, 755–768.e755.

Deleage, C., Wietgrefe, S.W., Del Prete, G., Morcock, D.R., Hao, X.P., Piatak, M., Jr., Bess, J., Anderson, J.L., Perkey, K.E., Reilly, C., et al. (2016). Defining HIV and SIV reservoirs in lymphoid tissues. Pathog. Immun. *1*, 68–106.

Deleage, C., Immonen, T.T., Fennessey, C.M., Reynaldi, A., Reid, C., Newman, L., Lipkey, L., Schlub, T.E., Camus, C., O'Brien, S., et al. (2019). Defining early SIV replication and dissemination dynamics following vaginal transmission. Sci. Adv. *5*, eaav7116.

Domanska, D., Majid, U., Karlsen, V.T., Merok, M.A., Beitnes, A.R., Yaqub, S., Baekkevold, E.S., and Jahnsen, F.L. (2022). Single-cell transcriptomic analysis of human colonic macrophages reveals niche-specific subsets. J. Exp. Med. *219*.

Doyle, C.M., Vine, E.E., Bertram, K.M., Baharlou, H., Rhodes, J.W., Dervish, S., Gosselink, M.P., Di Re, A., Collins, G.P., Reza, F., et al. (2021). Optimal isolation protocols for examining and interrogating mononuclear phagocytes from human intestinal tissue. Front. Immunol. *12*, 727952.

Eugenin, E.A., and Berman, J.W. (2016). Improved methods to detect low levels of HIV using antibody-based technologies. Methods Mol. Biol. *1354*, 265–279.

Eugenin, E.A., Gaskill, P.J., and Berman, J.W. (2009). Tunneling nanotubes (TNT) are induced by HIV-infection of macrophages: a potential mechanism for intercellular HIV trafficking. Cell. Immunol. *254*, 142–148.

Felts, R.L., Narayan, K., Estes, J.D., Shi, D., Trubey, C.M., Fu, J., Hartnell, L.M., Ruthel, G.T., Schneider, D.K., Nagashima, K., et al. (2010). 3D visualization of HIV transfer at the virological synapse between dendritic cells and T cells. Proc. Natl. Acad. Sci. USA *107*, 13336–13341.

Fenton, T.M., Jorgensen, P.B., Niss, K., Rubin, S.J.S., Morbe, U.M., Riis, L.B., Da Silva, C., Plumb, A., Vandamme, J., Jakobsen, H.L., et al. (2020). Immune profiling of human gut-associated lymphoid tissue identifies a role for isolated

lymphoid follicles in priming of region-specific immunity. Immunity *52*, 557–570.e556.

Ganor, Y., Zhou, Z., Tudor, D., Schmitt, A., Vacher-Lavenu, M.C., Gibault, L., Thiounn, N., Tomasini, J., Wolf, J.P., and Bomsel, M. (2010). Within 1 h, HIV-1 uses viral synapses to enter efficiently the inner, but not outer, foreskin mucosa and engages Langerhans-T cell conjugates. Mucosal Immunol. *3*, 506–522.

Garcia, E., Pion, M., Pelchen-Matthews, A., Collinson, L., Arrighi, J.F., Blot, G., Leuba, F., Escola, J.M., Demaurex, N., Marsh, M., et al. (2005). HIV-1 trafficking to the dendritic cell-T-cell infectious synapse uses a pathway of tetraspanin sorting to the immunological synapse. Traffic *6*, 488–501.

Gillgrass, A., Wessels, J.M., Yang, J.X., and Kaushic, C. (2020). Advances in humanized mouse models to improve understanding of HIV-1 pathogenesis and immune responses. Front. Immunol. *11*, 617516.

Gupta, P., Collins, K.B., Ratner, D., Watkins, S., Naus, G.J., Landers, D.V., and Patterson, B.K. (2002). Memory CD4(+) T cells are the earliest detectable human immunodeficiency virus type 1 (HIV-1)-infected cells in the female genital mucosal tissue during HIV-1 transmission in an organ culture system. J. Virol. *76*, 9868–9876.

Gurney, K.B., Elliott, J., Nassanian, H., Song, C., Soilleux, E., McGowan, I., Anton, P.A., and Lee, B. (2005). Binding and transfer of human immunodeficiency virus by DC-SIGN+ cells in human rectal mucosa. J. Virol. *79*, 5762–5773.

Hladik, F., Sakchalathorn, P., Ballweber, L., Lentz, G., Fialkow, M., Eschenbach, D., and McElrath, M.J. (2007). Initial events in establishing vaginal entry and infection by human immunodeficiency virus type-1. Immunity *26*, 257–270.

Imle, A., Kumberger, P., Schnellbacher, N.D., Fehr, J., Carrillo-Bustamante, P., Ales, J., Schmidt, P., Ritter, C., Godinez, W.J., Muller, B., et al. (2019). Experimental and computational analyses reveal that environmental restrictions shape HIV-1 spread in 3D cultures. Nat. Commun. *10*, 2144.

Jackson, H.W., Fischer, J.R., Zanotelli, V.R.T., Ali, H.R., Mechera, R., Soysal, S.D., Moch, H., Muenst, S., Varga, Z., Weber, W.P., et al. (2020). The single-cell pathology landscape of breast cancer. Nature *578*, 615–620.

Keren, L., Bosse, M., Marquez, D., Angoshtari, R., Jain, S., Varma, S., Yang, S.R., Kurian, A., Van Valen, D., West, R., et al. (2018). A structured tumor-immune microenvironment in triple negative breast cancer revealed by multiplexed ion beam imaging. Cell *174*, 1373–1387.e1319.

Kim, J., Koo, B.K., and Knoblich, J.A. (2020). Human organoids: model systems for human biology and medicine. Nat. Rev. Mol. Cell Biol. *21*, 571–584.

Kobayashi, N., Takahashi, D., Takano, S., Kimura, S., and Hase, K. (2019). The roles of peyer's Patches and microfold cells in the gut immune system: relevance to autoimmune diseases. Front. Immunol. *10*, 2345.

Koh, W.H., Lopez, P., Ajibola, O., Parvarchian, R., Mohammad, U., Hnatiuk, R., Kindrachuk, J., and Murooka, T.T. (2020). HIV-captured DCs regulate T cell migration and cell-cell contact dynamics to enhance viral spread. iScience *23*, 101427.

Langman, J.M., and Rowland, R. (1986). The number and distribution of lymphoid follicles in the human large intestine. J. Anat. *149*, 189–194.

Lewis, S.M., Asselin-Labat, M.L., Nguyen, Q., Berthelet, J., Tan, X., Wimmer, V.C., Merino, D., Rogers, K.L., and Naik, S.H. (2021). Spatial omics and multiplexed imaging to explore cancer biology. Nat. Methods *18*, 997–1012.

MacKinnon, D.P., Krull, J.L., and Lockwood, C.M. (2000). Equivalence of the mediation, confounding and suppression effect. Prev. Sci. *1*, 173–181.

Maric, D., Grimm, W.A., Greco, N., McRaven, M.D., Fought, A.J., Veazey, R.S., and Hope, T.J. (2021). Th17 T cells and immature dendritic cells are the preferential initial targets after rectal challenge with a simian immunodeficiency virus-based replication-defective dual-reporter vector. J. Virol. *95*, e0070721.

McDonald, D., Wu, L., Bohks, S.M., KewalRamani, V.N., Unutmaz, D., and Hope, T.J. (2003). Recruitment of HIV and its receptors to dendritic cell-T cell junctions. Science *300*, 1295–1297.

Nasr, N., Lai, J., Botting, R.A., Mercier, S.K., Harman, A.N., Kim, M., Turville, S., Center, R.J., Domagala, T., Gorry, P.R., et al. (2014). Inhibition of two temporal phases of HIV-1 transfer from primary Langerhans cells to T cells: the role of langerin. J. Immunol. *193*, 2554–2564.

Nikolic, D.S., Lehmann, M., Felts, R., Garcia, E., Blanchet, F.P., Subramaniam, S., and Piguet, V. (2011). HIV-1 activates Cdc42 and induces membrane extensions in immature dendritic cells to facilitate cell-to-cell virus propagation. Blood *118*, 4841–4852.

Pilcher, C.D., Joaki, G., Hoffman, I.F., Martinson, F.E., Mapanje, C., Stewart, P.W., Powers, K.A., Galvin, S., Chilongozi, D., Gama, S., et al. (2007). Amplified transmission of HIV-1: comparison of HIV-1 concentrations in semen and blood during acute and chronic infection. AIDS *21*, 1723–1730.

Prevedel, L., Ruel, N., Castellano, P., Smith, C., Malik, S., Villeux, C., Bomsel, M., Morgello, S., and Eugenin, E.A. (2019). Identification, localization, and quantification of HIV reservoirs using microscopy. Curr. Protoc. Cell Biol. *82*, e64.

Renault, C., Veyrenche, N., Mennechet, F., Bedin, A.S., Routy, J.P., Van de Perre, P., Reynes, J., and Tuaillon, E. (2022). Th17 CD4+ T-cell as a preferential target for HIV reservoirs. Front. Immunol. *13*, 822576.

Rhodes, J.W., Tong, O., Harman, A.N., and Turville, S.G. (2019). Human dendritic cell subsets, ontogeny, and impact on HIV infection. Front. Immunol. *10*, 1088.

Rhodes, J.W., Botting, R.A., Bertram, K.M., Vine, E.E., Rana, H., Baharlou, H., Vegh, P., O'Neil, T.R., Ashhurst, A.S., Fletcher, J., et al. (2021). Human anogenital monocyte-derived dendritic cells and langerin+cDC2 are major HIV target cells. Nat. Commun. *12*, 2147.

Schapiro, D., Jackson, H.W., Raghuraman, S., Fischer, J.R., Zanotelli, V.R.T., Schulz, D., Giesen, C., Catena, R., Varga, Z., and Bodenmiller, B. (2017). histoCAT: analysis of cell phenotypes and interactions in multiplex image cytometry data. Nat. Methods *14*, 873–876.

Stieh, D.J., Matias, E., Xu, H., Fought, A.J., Blanchard, J.L., Marx, P.A., Veazey, R.S., and Hope, T.J. (2016). Th17 cells are preferentially infected very early after vaginal transmission of SIV in macaques. Cell Host Microbe *19*, 529–540.

Trifonova, R.T., Bollman, B., Barteneva, N.S., and Lieberman, J. (2018). Myeloid cells in intact human cervical explants capture HIV and can transmit it to CD4 T cells. Front. Immunol. *9*, 2719.

Unthank, J.L., and Bohlen, H.G. (1988). Lymphatic pathways and role of valves in lymph propulsion from small intestine. Am. J. Physiol. *254*, G389–G398.

Vine, E.E., Rhodes, J.W., Warner van Dijk, F.A., Byrne, S.N., Bertram, K.M., Cunningham, A.L., and Harman, A.N. (2022). HIV transmitting mononuclear phagocytes; integrating the old and new. Mucosal Immunol. *15*, 542–550.

Wang, J.H., Janas, A.M., Olson, W.J., and Wu, L. (2007). Functionally distinct transmission of human immunodeficiency virus type 1 mediated by immature and mature dendritic cells. J. Virol. *81*, 8933–8943.

Wang, J.H., Wells, C., and Wu, L. (2008). Macropinocytosis and cytoskeleton contribute to dendritic cell-mediated HIV-1 transmission to CD4+ T cells. Virology *381*, 143–154.

Whitney, J.B., Hill, A.L., Sanisetty, S., Penaloza-MacMaster, P., Liu, J., Shetty, M., Parenteau, L., Cabral, C., Shields, J., Blackmore, S., et al. (2014). Rapid seeding of the viral reservoir prior to SIV viraemia in rhesus monkeys. Nature *512*, 74–77.

Wizenty, J., Ashraf, M.I., Rohwer, N., Stockmann, M., Weiss, S., Biebl, M., Pratschke, J., Aigner, F., and Wuensch, T. (2018). Autofluorescence: a potential pitfall in immunofluorescence-based inflammation grading. J. Immunol. Methods *456*, 28–37.

Yu, H.J., Reuter, M.A., and McDonald, D. (2008). HIV traffics through a specialized, surface-accessible intracellular compartment during trans-infection of T cells by mature dendritic cells. PLoS Pathog. *4*, e1000134.

Zhou, Z., Xu, L., Sennepin, A., Federici, C., Ganor, Y., Tudor, D., Damotte, D., Barry Delongchamps, N., Zerbib, M., and Bomsel, M. (2018). The HIV-1 viral synapse signals human foreskin keratinocytes to secrete thymic stromal lymphopoietin facilitating HIV-1 foreskin entry. Mucosal Immunol. *11*, 158–171.

STAR★METHODS

KEY RESOURCES TABLE

REAGENT or RESOURCE	SOURCE	IDENTIFIER
Antibodies		
Sheep Polyclonal anti-FXIIIA	Affinity Biologicals	Cat: SAF13A-AP
Rabbit monoclonal anti-CD11c (clone EP1347Y)	Abcam	Cat# ab52632; RRID: AB_2129793
Mouse monoclonal anti-CD3 (clone F7.2.38)	Abcam	Cat# ab181724; RRID: AB_302587
Rabbit anti-CD4 (clone EPR6855)	Abcam	Cat# ab181724; RRID: AB_2864377
Rabbit anti E-Cadherin-AF647 (clone 24E10)	Cell Signal	Cat# 9835; RRID: AB_10828228
Donkey anti-sheep-AF488	Invitrogen	Cat: A-11015
Donkey anti-rabbit-AF647	Invitrogen	Cat: A-31573
Donkey anti-mouse-DyLight755	Invitrogen	Cat: SA5-10171
HLA-DR BUV395 (L243)	Biolegend	N/A
HLA-DR PerCP (AC122)	Miltenyi Biotec	Cat# 130-108-056; RRID: AB_2661330
CD19 BV750 (HI819)	Biolegend	N/A
CD19 APC Vio770 (L719)	Miltenyi Biotec	N/A
CD4 BV785 (OKT4)	Biolegend	Cat# 317442; RRID: AB_2563242
CD4 BV650 (OKT4)	Biolegend	Cat# 317436; RRID: AB_2563050
CD3 BUV496 (UCHT1)	BD	Cat# 612940; RRID: AB_2870222
CD3 APC Vio770 (REA613)	Miltenyi Biotec	Cat# 130-113-698; RRID: AB_2726239
CD14 BUV737 (M5E2)	BD	Cat# 612763; RRID: AB_2870094
CD14 BV421 (M5E2)	Biolegend	BioLegend Cat# 301830; RRID: AB_10959324
CD11c BB515 (B-ly6)	BD	Cat# 564490; RRID: AB_2744273
CD11c PE CF594 (B-ly6)	BD	Cat# 562393; RRID: AB_11153662
p24-PE (KC57)	Beckman Coulter	Cat# 6604667; RRID: AB_1575989
p24-APC (28b7)	Medimabs	Cat: MM-0289-APC
Bacterial and virus strains		
HIV- BaL	HEK293T transfection with $pWT/_{BaL}$	N/A
HIV- Z3678M	HEK293T transfection with $pHIV_{Z3678MTF}$	N/A
Biological samples		
Human colorectal tissue	Department of Colorectal Surgery Westmead Hospital	N/A
Critical commercial assays		
RNAscope 2.5HD Reagent Kit-RED	ACD Bio	Cat: 322360
sulfo-Cyanine7 antibody labelling kit	Lumiprobe	Cat: 5321–10rxn
Dead Cell Removal Kit	Miltenyi Biotec	Cat: 130-090-101
EasySep Human CD4+ T Cell Enrichment Kit	StemCell Technologies, Vancouver, Canada	Cat: 19052
Human CD45 Microbead Enrichment Kit	Miltenyi Biotec	Cat# 130-045-801; RRID: AB_2783001
Human CD14 Microbead Enrichment Kit	Miltenyi Biotec	Cat# 130-050-201; RRID: AB_2665482
Human CD19 Microbead Enrichment Kit	Miltenyi Biotec	Cat# 130-050-301; RRID: AB_2848166
Deposited data		
All data to reproduce figures in this paper	This study	https://doi.org/10.5281/zenodo.6992156
Experimental models: Cell lines		
HEK293T Cells	ATCC	N/A
HeLa-derived TZM-bls	NIH AIDS Reagent Program	John Kappes and Xiaoyun Wu
SUPT1.CCR5-CL.30 cells	Human Non-Hodgkin's T lymphocyte Lymphoma	James Hoxie, University of PA

(*Continued on next page*)

Continued		
REAGENT or RESOURCE	SOURCE	IDENTIFIER
Oligonucleotides		
custom probes targeting HIV-1_{BaI} (85zz pairs spanning base pairs 1144–8431)	ACD Bio	REF: 486631
custom probes targeting HIV_{Z3678M} (85zz pairs spanning base pairs 1149 – 8505)	ACD Bio	REF: 811791
Recombinant DNA		
$pWT/_{BaL}$	NIH AIDS Research and Reference Reagent Program	Dr. Bryan R. Cullen
$pHIV_{Z3678MTF}$	Gift from Eric Hunter	Genbank: KR820393
Software and algorithms		
Image processing: Huygens Professional 18.10	Scientific Volume Imaging	N/A
Image Processing: Fiji (Madison Version)	ImageJ	N/A
Image processing: Autofluorescence Identifier 'AFid' software	(Baharlou et al., 2020)	https://ellispatrick.github.io/AFid
Data Extraction: MATLAB 2017b	Mathworks	N/A
Analysis code to reproduce figures in this paper	This study: https://doi.org/10.5281/zenodo.6992156	https://github.com/heevaBaharlou/HIVImageAnalysis
SpicyR package	Bioconductor	10.18129/B9.bioc.spicyR
FlowJo (Treestar)	FlowJo (Treestar).	N/A
R programming language	GNU	N/A
Other		
Schematics were created with Biorender	Biorender	Agreement number: HX23I22GBL

RESOURCE AVAILABILITY

Lead contact

Further information and requests for resources and reagents should be directed to and will be fulfilled by the lead contact, Andrew Harman (andrew.harman@sydney.edu.au).

Materials

This study did not generate new unique reagents.

Data and code availability

- Raw image data and the processed spreadsheet used for analysis have been deposited at Zenodo at https://doi.org/10.5281/zenodo.6992156 (Baharlou et al., 2022) and are publicly available as of the date of publication. Flow cytometry data reported in this paper will be shared by the lead contact upon request.
- All original code and instructions for image processing/analysis is available at GitHub (https://github.com/heevaBaharlou/HIVImageAnalysis) and deposited at Zenodo at https://doi.org/10.5281/zenodo.6992156 (Baharlou et al., 2022).
- Any additional information required to reanalyze the data reported in this paper is available from the lead contact upon request.

EXPERIMENTAL MODEL AND SUBJECT DETAILS

Human subjects

Healthy human colorectal tissue was obtained within 15 min of resection from patients undergoing surgical intervention for diverticulitis or colorectal cancer. Only healthy tissue distal to the site of disease process were used for this study. Details on patient age and sex are provided in Table S1. This study was approved by the Western Sydney Local Area Health District (WSLHD) Human Research Ethics Committee (HREC); reference number HREC/2013/8/4.4(3777) AU RED HREC/13/WMEAD/232. Written consent was obtained from all donors.

Cell lines

Both human embryonic kidney-derived 293T (HEK293T Cells) and HeLa-derived TZM-bls were cultured in Dulbecco's Modified Eagle Medium (Lonza) with 10% Fetal Calf Serum (FCS) (Lonza) (DMEM10) at 37°C/5% CO_2 and passaged using TrypLE express

(Gibco) dissociation at a 1:10 dilution three times a week and 1:12 dilution twice a week, respectively. SUPT1.CCR5-CL.30 cells were maintained in RPMI (Lonza) with 10% FCS (RF10) at 37°C/5% CO_2 and passaged at a 1:10 dilution twice per week.

METHOD DETAILS

HIV-1 virus production

Lab-adapted (HIV_{BaL}) or transmitted founder (HIV_{Z3678M}) strains were produced by transfection using a previously described protocol (Bertram et al., 2019a). 1.6×10^7 HEK293T cells were seeded in a T150 flask (Becton Dickinson, Franklin Lakes, New Jersey, USA) and transfected with 80ug of $pWT/_{BaL}$ or $pHIV_{Z3678MTF}$ plasmid DNA. The following reaction mixture (all from Sigma-Aldrich) was prepared separately and added in addition to the plasmid DNA: 10μL 0.15M Na_2HPO_4 (pH 7.1), 128uL 2M $CaCl_2$, 1 mL Hepes-buffered saline (280 mM NaCl, 50 mM HEPES, pH 7.1), 1 mL (1 mM Tris, 0.1 mM EDTA, pH 8.0), all diluted in 15 mL DMEM10 (Lonza). Culture media was replaced the next day with DMEM10 and cells cultured for a further 2 days, after which media was collected, centrifuged (1600g, 20min) and the resultant supernatant concentrated (3000g, 20min) to 1mL using 300kDa filters (Vivaspin 20, Sartorius, Göttingen, Germany). High titer stocks for HIV_{BaL} were achieved by infection of the SUPT1 T cell line. Stocks were depleted of macrovesicles by adding 18mL viral supernatant to 2mL CD45 magnetic beads (Miltenyi Biotech) for 2h prior to filtering through an LS column (Miltenyi Biotech). The resultant CD45- HIV_{BaL} supernatant as well as HIV_{Z3678M} were under-layed with 1mL of 20% sucrose and ultracentrifuged (100,000g, 4°C, 1.5h, Beckman Optima XL-100 K, 70Ti rotor) to further concentrate viral stocks. This method yielded viral titers between 10^8–10^9, as measured by 50% tissue culture infective dose ($TCID_{50}$)/mL on TZM-bl cells by LTR β-galactosidase reporter gene expression following one round of infection. Briefly, serial dilutions of viral stocks were performed on plated TZM-bls (37°C, 3 days), followed by media removal, addition of 50ul X-gal solution and incubation for 1h at 37°C. Wells were then diluted with 50ul of 4% PFA and incubated for a further 20min at room temperature (RT), followed by solution removal and EliSPOT imaging. The Spearman & Kärber algorithm was used for $TCID_{50}$ measurements. Virus aliquots were stored at 80°C. Endotoxins (*Limulus* amebocyte lysate assay; Sigma), TNF-α, IFN-α, and IFN-β (Enzyme-linked immunosorbent assay (ELISA) were all below the limit of detection.

Tissue digestion

To perform HIV-uptake (Figure 3F) and co-culture/transfer assays (Figures 6F and 6G), we extracted HIV target cells from human colorectal tissue. Underlying fat and mesentery were removed using a scalpel and forceps and remaining tissue cut into ~5mm^2 pieces. Surface epithelium and mucus was stripped by two incubations in RPMI with 10% FCS, 0.3% DTT (Sigma) and 2mM EDTA (Sigma) (15min, 37°C). Tissue was washed in DPBS and underwent two incubations in 20mL RPMI with 0.3% Collagenase IV (Worthington) and 0.5% DNase (Sigma) (30min, 37°C) to liberate cells which were then passed through a 100μm cell strainer and washed twice in DPBS. Cells were resuspended in 35mL RPMI, under-layed with 15mL Ficoll-Paque (GE Healthcare) and centrifuged (400g, 20min, no brakes). Buffy coats were collected and washed twice in DPBS. Red Cell Lysis buffer (All Sigma: 150 mM ammonium chloride (v/v), 10mM potassium bicarbonate (v/v), 0.1 mM EDTA (v/v) in ddH20) was used to remove remaining red blood cells as per the manufacturer's instructions.

HIV uptake assay

Following our tissue digestion protocol (see above), liberated cells underwent positive selection for CD45+ cells (Miltenyi Biotec). 5×10^5 cells in 150ul of DC Culture Media were then treated with HIV_{Bal} (MOI = 5, 2h, 37°C) or PBS (mock). Cells were then washed three times in DPBS, 200ul of DPBS, stained with 0.05ul FVS700 for 30min at 4°C, washed in FACS wash (1% FCS (v/v), 2 mM EDTA, 0.1% sodium azide (w/v) in PBS) and 10ul Brilliant Stain Buffer (BD) added. Cells were then incubated with an antibody panel for 30min at 4°C with the final volume made to 50ul. The antibody panel included Biolegend: 1ul HLA-DR BUV395 (L243), 1ul CD19 BV750 (HI819), 2.5ul CD4 BV786 (OKT4); BD: 5ul CD3 BUV496 (UCHT1), 2.5ul CD14 BUV737 (M5E2), 1.5ul CD11c BB515 (B-ly6). Cells were washed in FACS wash, permeabilised with 100ul Cytofix/Cytoperm (BD) for 20min at RT and washed in Perm Wash (1% FCS (v/v), 1% BSA (w/v), 0.1% saponin (w/v), 0.1% sodium azide (w/v) in PBS) Cells were resuspended in 50ul Perm Wash and underwent intracellular staining with antibodies Beckman Coulter: p24-PE (KC57) and Medimabs: p24-APC (28b7) for 30min at RT. Cells were again washed in Perm Wash and HIV expression assessed by dual p24 expression using an LSRFortessa (BD). P24 expression was measured by gMFI and dual p24+ positive cells were defined as HIV+ cells as per (Bertram et al., 2019a; Rhodes et al., 2021). Mock treated cells were used to set the gates to minimize background staining interference.

Target cell selection and sorting

Following tissue digestion (see above), liberated cells were positively selected for CD45+ cells as per the manufacturer's instructions (EasySep Human CD45+ Cell Enrichment Kit, StemCell Technologies) using a QuadroMACS separator with LS columns. 2.5×10^6 cells were resuspended in 200ul of DPBS, stained with 0.05ul FVS700 for 30min at 4°C, washed in FACS wash and 10ul Brilliant Stain Buffer added. Our antibody sort panel was added for 30min at 4°C with the final volume made to 50ul. The sort panel included Miltenyi: 2.5ul CD3 APC Vio770 (REA613), 2.5ul CD19 APC Vio770 (L719), 1ul HLA-DR PerCP (AC122); Biolegend: 2ul CD4 BV650 (OKT4); BD: 1.5ul CD11c PE CF594 (B-ly6), 2.5ul CD14 BV421 (M5E2). Cells were then washed twice in FACS wash and once in pre-sort buffer (BD). 1mL of pre-sort buffer was used to resuspend cells which were then filtered using a 100μm cell strainer just prior

to sorting on either the BDInflux (BD) or BDAriaIII (BD) cell sorters. CD4+ T cells were defined as live CD3+CD4+, Dendritic Cells as live HLA-DR+CD3-CD19-CD14-CD11c+ and Macrophages as live HLA-DR+CD3-CD19-CD14+. Sorted cells were placed in FACS tubes with 500ul of DC Culture Media and kept at 4°C until co-culture/transfer assay setup as described in the sections below.

HIV co-culture assay

Sorted DCs, macrophages and CD4+ T cells were plated as follows: CD4+ T cells alone, DCs with CD4+ T cells (1:10 ratio), macrophages with CD4+ T Cells (1:10 ratio). Cultures were topped to 150ul with DC Culture Media and treated with HIV_{Z3678M} (MOI = 1, 2h, 37°C). An additional mock treated CD4+ T cell culture was maintained as a control. Cells were then washed three times in DC Culture Media, re-suspended in 200ul of DC Culture Media with 0.02% Normocin (InvivoGen) and cultured for 3 days at 37°C. HIV infection of CD4+ T cells was determined by p24 expression using flow cytometry as described in the section on 'HIV assessment by Flow Cytometry'.

HIV transfer assay

Sorted DCs and macrophages as well as activated PBMC-derived CD4+ T cells (see section below) were plated in individual wells in 150ul DC Culture media, then exposed to HIV_{Z3678M} (MOI = 1, 2h, 37°C). An additional mock treated activated CD4+ T cell culture was maintained as a control. Cells were then washed three times in DC Culture Media and resuspended in 200ul of DC Culture Media with 0.02% Normocin. Activated CD4+ T cells were then added to DC and Macrophage cultures at a 2:1 ratio and cultured for 3 days at 37°C. HIV infection of CD4+ T cells was determined by p24 expression using flow cytometry as described in the section on 'HIV assessment by Flow Cytometry'.

HIV assessment by flow cytometry

Cells cultured with HIV were washed in DPBS, resuspended in 200ul, stained with FVS700 for 20min at 4°C and washed with FACS wash. Cells were stained with Miltenyi: CD3 APC-Vio770 (REA613) for 30min at 4°C, washed twice in FACS wash, permeabilized with 100ul Cytofix/Cytoperm for 20min at RT and washed in Perm Wash. Cells were resuspended in 50ul Perm Wash and underwent intracellular staining with antibodies Beckman Coulter: 1ul p24-PE (KC57) and Medimabs: 1ul p24-APC (28b7) for 30min at RT. Cells were again washed in Perm Wash and HIV expression assessed by dual p24 expression using an LSRFortessa.

PBMC-derived CD4+ T cell isolation

Transfer assays (Figure 6G) were performed using allogenic activated CD4+ T cells selected from peripheral blood mononuclear cells (PBMCs). PBMCs were derived from leukoreduction system chambers (LRSC) (Australian Red Cross Blood Service), on the same day as platelet donation. LRSCs were diluted 1:5, distributed across Falcon tubes with 35mL in each tube, then under-layed with 15mL Ficoll-Paque and centrifuged (400g, 20min, no brakes). Buffy coats were collected and washed ×2 in DPBS. Red Cell Lysis buffer was used to remove remaining red blood cells as per the manufacturer's instructions. CD4+ T cells were selected using a CD4 selection kit (StemCell Technologies) and activated by culturing 1×10^6 cells/mL for 3 days at 37°C in RPMI supplemented with 10% FCS, 5 mg/mL PHA (Sigma) and 150 IU/mL IL-2 (Peprotech). Cells were transferred to cryovials containing FCS with 10% DMSO, placed in a CoolCell (Corning) and stored at −80°C.

HIV explant infection

Human colorectal tissue was obtained within 15 min of surgical resection. Underlying fat and mesentery were removed using a scalpel and forceps and tissue spread out in a Petri dish with the mucosal surface face-up. Gel-foam sponges (Pfizer) were cut into $1cm^2$ pieces (one for each explant), placed in the well of a 24-well plate and soaked in culture media consisting of 10μM HEPES (Gibco), non-essential amino acids (Gibco), 1 mM sodium pyruvate (Gibco), 50μM 2-Mercaptoethanol (Gibco), 10ug/mL Gentamycin (Gibco), 10% FCS (Lonza), all diluted in RPMI-1640 (Lonza). Here after this is referred to as 'DC Culture Media'. Sponges were left to soak whilst tissue was further processed. As previously described (Doyle et al., 2021; Fenton et al., 2020) a dissection light microscope was used to select appropriate placement of cloning cylinders for the topical application of HIV. Appropriate areas were defined as containing visible lymphoid aggregates and being free of any signs of trauma. Once an appropriate area was located, an 8mm cloning cylinders (Sigma-Aldrich) was lightly coated on one side with histoacryl surgical glue (B Braun) using a fine paint brush and carefully placed over the region. 500ul of PBS was then added to the cloning cylinder to prevent the tissue surface from drying out and to hasten setting of the surgical glue. This step is critical as excess glue can slowly spread over time from the cylinder edge and cover the tissue surface thus preventing viral entry. Once all cylinders were placed, tissue within cylinders were checked again to ensure they were free of glue. 1 or 2 selected regions did not have cylinders placed but were resected with a scalpel as a $1cm^2$ area and fixed in 4% PFA (diluted in PBS) (electron microscopy sciences) for 18h. These samples were used to analyze target cell distribution in fresh uninfected colorectal tissue (Figure 2). The Petri dish was then filled with PBS so as to just cover its surface, which reduced friction and the likelihood of displacement of the cylinders during cutting and lifting of explants. Soaked gel-foam sponges were then distributed across the 24-well plate. The perimeter surrounding each cloning cylinder was then cut, after which forceps were used to lift explants and place them on the sponges. Wells were then filled with DC Culture Media to the level of the tissue. A final quality check for cloning cylinder sealing was performed by ensuring that the previously applied PBS was still present and at the same level across explants. Solutions were removed from all cylinders and either 100ul PBS (mock), or a $TCID_{50}$ of 70,000 (diluted in 100ul PBS) of lab adapted (HIV_{BaL}) or transmitted founder (HIV_{Z3678M}) strains applied to the inner chamber of

cloning cylinders for 2h at 37°C. The time point of 2h was chosen as it allowed sufficient viral penetration into the tissue and was short enough that the explants did not start to degrade. Indeed, initial optimizations with 30min and 6h timepoints showed insufficient viral penetration past the epithelial surface and early signs of tissue degradation respectively (data not shown). It should be noted that degradation as early as 6h was likely due to the large size (~1cm^2) of our explants. A $TCID_{50}$ of 70,000 was selected as it is comparable to peak levels of infectious virus found in semen during the acute stage (Pilcher et al., 2007). Supernatant from inner chamber, as well as the DC Culture Media below were collected and stored at 80°C for assessment of HIV leakage from cylinders during the culture period (Figure S3O). Explants were then washed ×3 with 500ul PBS to remove excess HIV from the mucosal surface prior to cylinder removal and tissue fixation in 4% PFA (diluted in PBS) for 18h.

Tissue embedding and sectioning

After fixation, explants were removed and trimmed with a scalpel along the impression left by the cloning cylinder during the culture period. This ensured that only areas exposed to virus remained. Explants were kept in 70% ethanol prior to embedding in paraffin. Tissues were then embedded flat so that the mucosal surface faced away from the sectioning surface of the paraffin block. This ensured that the thin mucosal surface would not accidently be trimmed away whilst sectioning. 4μm transverse sections were taken through the entire tissue, from the submucosal side to the end of mucosa, and placed on Superfrost Ultra Plus Adhesion Slides (Thermo Scientific) Sections were stored in the dark at RT until staining.

RNAScope

Detection of HIV RNA was performed using RNAscope as previously described (Bertram et al., 2019a; Deleage et al., 2016; Rhodes et al., 2021) using the RNAscope 2.5HD Reagent Kit-RED′ with custom probes targeting HIV-1_{Bal} or HIV_{Z3678M}. In the protocol that follows, reagents included in the 'RNAscope 2.5HD Reagent Kit-RED' are indicated. Unless otherwise written, wash steps were for 2min on a rotator set to low and incubations were carried out in a hybridization oven (HybEZ Hybridization System (220VAC), ACD Bio). 4μm paraffin sections were baked at 60°C for 1h and dewaxed by sequentially submerging slides in xylene (2 × 2min) and 100% ethanol (2 × 2min). Slides were air-dried and antigen retrieval performed for 20min at 95°C using a pH9 buffer (RNAscope kit) and a decloaking chamber (Biocare). Sections were washed in TBS (Amresco, Cat: 0788), then Milli-Q H_2O, followed by dipping slides 3–5 times in 100% ethanol, leaving them to air dry and then encircling sections with a hydrophobic pen (RNAscope kit). Sections were then incubated with protease pre-treatment 3 (diluted 1:5 in PBS and kept ice-cold) (RNAscope kit) for 30min at 40°C. Sections were washed ×2 in Milli-Q H_2O and incubated with probes targeting HIV-1_{Bal} or HIV_{Z3678M} for 2h at 40°C. Sections were washed ×2 in RNAscope wash buffer (RNAscope kit). Signal from probes was then amplified using Amps 1–6 (RNAscope kit) which were added in sequence with ×2 washes in RNAscope wash buffer between Amps. Amp incubation times were as follows Amp 1 = 30 min at 40°C; Amp 2 = 15 min at 40°C; Amp 3 = 30 min at 40°C; Amp 4 = 15 min at 40°C; Amp 5 = 30 min at RT; Amp 6 = 15 min at RT. HIV RNA Signal was developed using Fast Red substrate made by mixing Red-B and Red-A (RNAscope kit) at a 1:75 ratio for 5min at RT, followed by washing in Milli-Q H_2O then TBS.

Cyclic immunofluorescence staining and image acquisition

Unless otherwise indicated all washes were 2 × 2min in TBS on rotator set to low and incubations were in a humidified chamber protected from light. Following RNAscope, sections were blocked for 30min at RT with blocking buffer (10% donkey serum (Sigma), 1% BSA (Sigma), 0.1% Saponin (Sigma), all diluted in TBS) and washed. Sections were incubated with sheep anti-FXIIIa and rabbit anti-CD11c antibodies (diluted in block buffer) overnight at 4°C, washed and donkey anti-sheep-AF488 (Invitrogen, Cat: A-11015) and donkey anti-rabbit-AF647 (Invitrogen, Cat: A-31573) antibodies added for 30min at RT. Sections were washed and further blocked for 30min at RT with block buffer with 10% rabbit serum (DAKO) to block excess binding sites from the donkey anti-rabbit antibodies. 0.5% PFA (diluted in PBS) was added for 15min at RT to fix blocking rabbit IgGs in place. Rabbit anti-CD4-Cy7 (Abcam, Cat: ab181724, conjugation with sulfo-Cyanine7 antibody labeling kit (lumiprobe, Cat: 5321–10rxn)) was then added overnight at RT and sections washed 3 × 5min in TBS. Sections were stained with 1ug/mL DAPI (diluted in TBS) (Thermo Scientific, Cat: 62248) for 3min at RT, washed then rinsed in Milli-Q water. Sections were mounted with SlowFade Diamond Antifade Mountant (Invitrogen, Cat: S36963) and cover-slipped (Menzel-Glaser 22 × 60 mm Coverslip, Thermo Scientific). Images were acquired as per the section below on 'Image Acquisition'. After imaging, slides were submerged in TBS until coverslips dissociated. Sections were then washed and treated with bleach solution (5% H2O2 (Sigma) and 20mM NaOH (Sigma) diluted diluted in PBS) for 1h with light (15 watt, 2700k light bulb, 5cm above sample). Sections were checked under the microscope to ensure signal removal from all channels, and subsequently washed and incubated with blocking buffer with 10% rabbit serum for 15min at RT, followed by washing in TBS. Rabbit E-Cadherin-AF647 (Cell Signal, Cat: 9835) and mouse anti-CD3 (Abcam, Cat: ab17143) were added overnight at RT. Sections were washed 3 × 5min in TBS and donkey anti-mouse-DyLight755 antibody (Invitrogen, Cat: SA5-10171) then added for 30min at RT. After washing 3 × 5min in TBS and rinsing in Milli-Q water slides were again mounted with SlowFade Diamond Antifade Mountant and imaged as described below.

Image acquisition

Images were acquired with a VS120 Slide Scanner equipped with an ORCA-FLASH 4.0 VS: Scientific CMOS camera (Olympus) and VS-ASW 2.9 software used for image acquisition and file conversion from vsi to tiff format. The entire tissue area was imaged using an

×20 objective (UPLSAPO 20X/NA 0.75, WD 0.6/CG Thickness 0.17) and select areas for representative images were acquired using an ×40 objective (UPLSAPO 40X/NA 0.95, WD 0.18/CG Thickness 0.11–0.23). For x40 images, Z-stacks were acquired 3.5μm above and below the plane of focus with 0.5μm step sizes. Channels used include: DAPI (Ex 387/11–25nm; Em: 440/40–25nm), FITC (Ex: 485/20–25nm; Em: 525/30–25nm), TRITC (Ex: 560/25–25 nm; Em: 607/36–25nm), Cy5 (Ex: 650/13–25 nm; Em: 700/75–75nm) and Cy7 (Ex: 710/75nm, Em: 810/90nm). All channels were checked, and antibodies titrated beforehand, to ensure against signal-spill over between channels.

QUANTIFICATION AND STATISTICAL ANALYSIS

Image deconvolution and registration

Huygens Professional 18.10 (Scientific Volume Imaging, The Netherlands, http://svi.nl) CMLE algorithm, with SNR: 20 and 40 iterations were used for deconvolution of both single plane images acquired at x20, and also ×40 Z-stacks. Images were aligned using the ImageJ plugin multiStackReg vs1.45 with the DAPI channel serving as a reference for alignment.

Autofluorescence removal

Colorectal tissue is prone to autofluorescence from many sources such as red blood cells, blood vessels, apoptotic cells, intrinsically autofluorescent cells etc. Our early analyzes showed this substantially interfered with cell phenotyping and we could not remove autofluorescence using commercial quenching kits without significantly reducing our staining intensity. As such we developed 'Autofluorescence Identifier' (AFid) which analyzes pixels from two input fluorescent channels and outlines autofluorescent objects (Baharlou et al., 2020). The code (https://ellispatrick.github.io/AFid) is implemented in MATLAB, R and Fiji. The Fiji version was used for this analysis. Pairs of channels compared were FXIIIA (on FITC) vs HIV RNA (on Texas Red) and HIV RNA vs CD11c. Autofluorescence masks were 'OR' combined and the resultant mask was used to exclude autofluorescent pixels (values set to 0) from images during data extraction as described below. The input parameters for AFid were as follows:

Threshold: Niblack
Min Area = 20 pixels.
Max Area = 100000 pixels.
Sigma = 2 pixels.
Correlation cut off = 0.6.
Number of clusters = 1.
Max Value to automate k = 0.
Glow Removal = Yes.
Expansion Sensitivity = 20 pixels.
*Above values were for image resolutions of 3 pixels per μm.

HIV spot segmentation

HIV RNA particles were segmented using a custom MATLAB script based on a previously described spot counting algorithm (Battich et al., 2013). First, a manual threshold of the HIV RNA channel was set to approximate areas of HIV stain. The IdentifySpots2D function by Battich et al. was then used to identify the number of spots. The detection threshold was set to 0.01 and deblending steps was set to 2. Identified spots were excluded if they did not overlap with the manually generated threshold mask in the first step.

Cell segmentation and Classification

Single cell segmentation was performed using a customized implementation of CellProfiler (Carpenter et al., 2006) in MATLAB (nucleiSegment.m, segRun.m function). Nuclei segmentation was performed by applying a local otsu filter to threshold the DAPI image and applying object-based watershed to identify boundaries. Objects with diameter between 3.3 and 16.7μm were kept. Masks of the CD3, CD11c and FXIIIa images were obtained by Gaussian blurring each image (sigma = 1.5) and performing a manual threshold to capture the full membrane. The nuclei are then classified based on the percentage overlap of each nuclei object with each membrane mask. A cell is classified as a T cell if the overlap with CD3 is >20%, classified as a DC if the overlap with CD11c is >20%, and classified as a macrophage if the overlap with FXIIIa is >40%. Finally, three separate labeled cell masks are obtained for each cell type by expanding the nuclei to fill the membrane one pixel at a time (expandNucleus.m). For example, a nucleus identified as a macrophage is expanded into the FXIIIa mask space. A schematic with further details is provided in (Figure S1C).

Tissue compartment segmentation

A manual threshold of the E-Cadherin stain was determined and nuclei (as segmented in the above section) belonging to this compartment were extracted using the BinaryReconstruct function in the 'Morphology' package in Fiji. The E-Cadherin and nuclei masks were then combined. The submucosa and lymphoid aggregates were manually outlined in Fiji and masks generated. The submucosa was defined as starting from the base of the crypts of Lieberkühn, whilst the border of lymphoid aggregates was determined by the increased density of CD11c and CD4 expressing DCs and T cells respectively. A mask of the whole tissue was then generated with a manually determined threshold. Subtracting the epithelium, lymphoid aggregates and submucosa from the whole tissue mask

provided a mask of the lamina propria. All masks were combined into a single image stack and assigned unique pixel values (eg, all epithelial pixels = 1, lamina propria pixels = 2 etc) so that they could be thresholded to extract data from each compartment.

Data extraction in Matlab

Data extraction was performed in MATLAB (toRunNoNeighbrs.m, to RunNeighbrs.m). The mean marker expression and number of HIV particles was identified. From the compartment masks, a cell was considered to be part of that compartment if the overlap with the compartment mask was >25%. Distances from the compartments and HIV were obtained by creating a distance map from these objects and measuring the minimum value of the distance map within each cell. For cells within the LAs, the distance from the LA border was also measured in a similar approach. Neighbors were generated using the approach described in (Schapiro et al., 2017). Finally, using the cell masks, the overlap between cells were also identified. All data were exported into a single csv file with rows as individual cells and columns as cell features such CD4 expression, HIV particle number, distance from LAs etc.

Analysis in R

All image analysis for this study was performed in R using the csv spreadsheet of cells and their features, generated as described in the previous section. Procedures for statistical analysis generating the results in this paper are described in the methods below and links to the source code are provided in the Key resources table. Donor and image numbers used for each analysis are indicated in figure legends.

HIV enrichment and association testing in cells

As the virus-cell interactions were from incoming viral particles and not those synthesized by the cell itself, some of the interactions observed were false positives due to random cell encounter with virus. We reasoned that the degree of background interactions for a given cell type would be proportional to the cell population's frequency in tissue. As such, measuring the percentage of total image HIV particles in each cell type, would largely reflect the relative abundance of each cell type. To get around this, we performed tests of association and enrichment, which are able to account for cell type abundance.

A Chi Square test of association was used to measure HIV enrichment in the grouped target cell population (DCs, macrophages, CD4+ T cells) in each image used for this study (Figure 3A). Here the expected number of HIV particles in target cells was determined by the proportion of all cells that comprised target cells. This showed that in most cases, HIV preferentially associates with the target cell population under study, rather than the undefined remaining cells in each image.

HIV enrichment was also calculated for specific populations. HIV enrichment was defined as the log2 transform of the percentage of virions associated with a cell type divided by the cell type's percentage of all cells (Figure 3C).

HIV enrichment testing in tissue compartments

The calculation of HIV enrichment was extended to measure preferential virus localization between LP and LA compartments, rather than between cell populations (Figures 4B and 4C). The 'expected' percentage of HIV particles in each compartment was based on the proportional area of these compartments. For example, a 5:1 ratio of LP to LA area means that, by random chance, we expect 80% of virions in the LP and 20% in LAs. The null hypothesis of there being no difference in HIV localization between compartments (i.e. it just follows the area ratio) is represented visually as the line y = x in Figure 5B. Consequently, the residual variance (Euclidean distance of datapoints from the line y = x) represents the magnitude of HIV enrichment in LAs (for points above the line) or the LP (for points below the line) in each image. Comparing residuals as in Figure 5D is therefore akin to comparing the propensity of HIV to localize to LAs or the LP, accounting for differences in area between these compartments. Important to note, only virions in the LP and LA were used for this analysis (i.e. EP and SM virions excluded). Accordingly, the reciprocal values on the x and y axes of Figure 5B are measurements for the LP. For example, the rightmost red data point is an image with 40% of the area comprised of LAs, and 60% of HIV in LAs. In this same image, 60% of the image area is comprised of LP which contains 40% of HIV.

Measuring HIV density across tissue compartments

HIV density was calculated for each tissue compartment separately. For a given compartment, HIV density was calculated using the top 10 images with the highest HIV density for that compartment. The HIV density of all compartments, calculated in this way, was then compared (Figure 4A). This approach was chosen to mitigate variation due to inter-image differences in HIV concentration, penetration depth and compartment proportions. For example, for a given donor the density of HIV in LAs often varies substantially by section due to difference in depth of viral penetration at 2h. This can lead to extremely high LA HIV densities in one section, and almost no virions in LAs in other sections from the same donor. In this case, using all images would mask the high HIV density observed in LAs in the earlier section. To get around this issue, we compared the highest observable HIV densities in each compartment, rather than simply measuring all compartments in all images.

Cellular spatial distribution within compartments

Measurement of cellular spatial distribution within compartments was performed using distance maps emanating from compartment borders (see section 'data extraction in Matlab'). Cell density was measured either in non-cumulative intervals (Figure 2D, left) or in just two regions defined as "-proximal" and "-distal" to the compartment border (Figure 2D right). The latter was mostly used for

statistical comparisons as comparing only two regions allowed for more observations (cells) per region and better statistical power. For EP, LP and SM, the non-cumulative intervals were linear (e.g., 0–20μm, 20–40μm … etc) (Figure 2D, left). To measure changes throughout LAs we used a different approach. To achieve comparable areas for each interval we assumed LAs to be spherical and hence circular in 2D. We then calculated the radial edges of each interval from the outer edge using the formula: 1 – sqrt (1 – k/n) where k = {1,2 … n-1} and n = max interval number. For a perfect circle this would derive intervals of equal area (Figures 4H and S3G–S3K).

Cellular gradients in response to HIV

Distance maps emanating from HIV particles (see section 'data extraction in Matlab') were used to analyze changes in cell density in the vicinity of HIV (Figure 5). The formation of increasing/decreasing cell density gradients in non-cumulative intervals from HIV particles was inferred as potential cell migration to/from HIV within a given compartment (Figure 5A).

Potential migration of LP target cells into the EP (Figures 5B and 5C) was assessed by measuring the cell density both near ($\leq$10μm from the EP-LP interface) and within HIV+ EP vs HIV- EP. A single relatively small interval of 10μm, rather than multiple intervals, was chosen due to the small space between epithelial crypts. If a comparative increase in the density of a target cell was observed both leading up to HIV+ EP and within the HIV+ EP itself, then we inferred this was likely the target cell migrating from the LP into the EP to sample HIV particles. We performed several filtering steps to remove potential interfering variables. In particular, HIV+ and HIV- EP cells could be located next to one another, and so HIV- EP were specifically selected as >50μm away from HIV+ EP. Additionally, many regions have more HIV in the LP than the EP, which could draw target cells away from HIV+ EP and toward HIV+ LP instead. To mitigate this effect images were binned into 100 × 100μm quadrats and only quadrats with more HIV particles in EP than LP were used for analysis. Finally, only images with at least one cell in each category were analyzed (e.g. at least one DC beneath each HIV+ and HIV- EP).

Potential migration of LP target cells into LAs (Figures 5D and 5E) was assessed by measuring the cell density in non-cumulative 50μm intervals from LAs and within LAs themselves. These measurements were split by whether LAs were HIV+ or HIV- and so only donors with both HIV+ and HIV- LAs were used in this analysis. We also compared the spatial distribution of target cells throughout intervals of HIV+ vs HIV- LAs (see 'Cellular spatial distribution within compartments' for methodology). This was to determine whether target cells clustered more toward the outer intervals of HIV+ LAs, which is where cells entering LAs from the LP would likely be located.

Analysis of pathways for submucosal HIV entry

HIV entry into the submucosa could only occur via either the LP or LAs, as these are the mucosal compartments directly overlying the submucosa. To analyze which pathway was most likely, we created linear models (*lm()* function in R) of submucosal HIV density as a function of LP HIV density, LA HIV density, or both (Figure 3I). Datapoints were individual explants, i.e., A compartment across all images from an explant was measured, producing a single value for that explant. The combined model showed that LA HIV density was the only significant predictor of SM HIV density. Although LP HIV density alone showed some predictive capacity that was borderline significant ($\beta = 0.54$, $p = 0.04$), this effect was diminished in the combined model. This was likely due to collinearity between LA and LP HIV density ($\beta = 0.71$, $p = 0.004$), causing the LP to transmit effects from the LA HIV density when attempting to predict SM HIV density. This assumes the direction of the association is that LP HIV density affects LA HIV density, and not the other way around. To explain why this assumption is likely true, consider two possible scenarios for HIV entry into the SM (1) LP → LA → SM and (2) LA → LP → SM. In each case, the middle variable is called the 'mediator' as it transmits the effects of the first variable to the last one. The criteria for a variable to be classed as a mediator are well established (Baron and Kenny, 1986) and are explained in simple by MacKinnon et al., (MacKinnon et al., 2000).

1. There must be a significant relationship between the independent variable and the dependent variable,
2. There must be a significant relationship between the independent variable and the mediating variable, and
3. The mediator must be a significant predictor of the outcome variable in an equation including both the mediator and the independent variable.

Referencing the equations in Figure 3I, we can see that only the LA variable satisfies these properties and can be classed as a mediator, indicating that the LP → LA → SM pathway is more likely.

SpicyR analysis

The R package 'SpicyR' (Canete et al., 2022) was used to analyze differential cell-cell localization between HIV and mock-treated samples in the EP, LP, LA and SM (Figure 6A). As HIV particles were only present in specific regions of the images from HIV-treated explants, we selected regions near HIV particles to compare to the mock sample. This is because the numerous HIV- regions would dilute the HIV-induced effects on cell-cell interactions when comparing to mock. The HIV-proximal region was defined as all cells within 30μm of HIV for the EP, LP and LA compartments, and 100μm for the SM due to the lower cell density in this compartment. As a control, HIV-distal regions (>30μm or 100μm) were compared to the mock sample. p values were centered at p = 0.01 which was the assigned cut-off for significant changes

for this analysis. Importantly, the SpicyR test function measures interactions of a cell type within a user specified radius around the cell. As the chosen radius is a possible source of variation in results, we tested multiple radii. We did this alongside testing multiple cut-offs to define the HIV-proximal region and found our results were robust to variation in these parameters (Figure S4A).

Temporal inference analysis

Having observed that LP target cells clustered away from the EP-interface we wanted to know whether this could be due to target cell migration away from the EP-interface in response to incoming HIV particles (Figure S4B). As we only performed a single 2h time point for our explants we devised a method of temporal inference to investigate this phenomenon. We observed different proportions of HIV in the EP and LP in different regions of our images. This was likely due to each region being at a different stage of HIV entry, with regions where most HIV was in EP representing early stages of HIV entry, and regions where most HIV was in LP representing later stages (as HIV would have already passed the EP barrier to enter the LP). As such we reasoned that we could use the relative proportion of HIV in EP vs LP as a proxy for 'early' vs 'later' stages of HIV entry. In particular, we divided images into 100 × 100μm windows with each window classified as HIV- windows (no HIV particles), 'early' (EP > LP HIV particle count) or 'late' (EP < LP HIV particle count) in terms of HIV entry. We then calculated the log2 fold change in LP target cell density in EP proximal ($\geq$10μm) vs distal regions (10–50μm) from either HIV- EP or HIV+ EP. A negative fold change indicates target cell enrichment in the distal region. If the magnitude of the negative fold change was higher in the distal region from HIV+ EP vs HIV- EP, then it means that HIV exposure to the tissue caused further relocation of the target cell away from the EP.

It's important to note that all windows contained a mixture of HIV+ and HIV- EP which is why the distance of LP target cells from each type of EP could be calculated for all windows. The HIV- EP was >50μm from HIV+ EP to minimize interference (as also described in '*Cellular gradients in response to HIV*'). The reason for measuring LP target cell distance from HIV- vs HIV+ EP is that it controlled for local fluctuations in LP target cell density, allowing us to better observe how a local region changes in early vs later stages of HIV entry. This is opposed to measuring cell distance from the EP in general and directly comparing changes in target cell density in early vs late windows. These windows would be in different regions and therefore could have vastly different steady-state target cell densities (therefore affecting the fold change measurements close and far from the EP).

HIV-transfer phenotype score

As HIV is present at the interface between cells during active viral transfer (Garcia et al., 2005; McDonald et al., 2003; Wang et al., 2007, 2008; Yu et al., 2008), neighboring cells engaged in transfer would both appear as HIV+ in our data. We sought to quantify the frequency of this phenotype between cell pairs, as a proxy for cellular engagement in viral transfer. This was achieved by employing a modified version of Neighborhood Analysis (Schapiro et al., 2017) and constructing a 'HIV-transfer phenotype score' from the results to estimate the degree to which a HIV+ cell increases the likelihood of nearby cells being HIV+, whilst controlling for possible confounders (Figure 6C). In particular, we first quantified the number of HIV+ and HIV- cell neighbors for HIV+ cells. The cell labels (locations) of HIV+ cells, rather than all cells, were randomized 999 times to generate a null distribution of HIV+ cell neighborhoods, against which the actual HIV+ cell neighborhood was compared to determine significant interactions ($p < 0.005$). Randomization was restricted to HIV+ cells to control for the background effect of HIV particles on the localization of cells in tissue (i.e. cells are already at an increased density in HIV+ regions). This is a key difference to standard neighborhood analysis which randomizes on all cells. This results in association scores for HIV+:HIV+ interactions (HIV+ cell with HIV+ neighbor) and 'HIV+:HIV-' interactions (HIV+ cell with HIV- neighbor), which was expressed as the percentage of all images showing significant interactions for the cell pair. Note that in this analysis, cells of the same type often appear to significantly interact with each other, which has been noted in previous spatial studies analyzing cell:cell interactions in tissue (Damond et al., 2019; Jackson et al., 2020; Keren et al., 2018).

Using these data we constructed a 'HIV-transfer phenotype score' which was defined as the difference in the frequency of 'HIV+:HIV+' interactions and 'HIV+:HIV-interactions. HIV+:HIV- interactions represent the moment before potential transfer and it's frequency is determined by all conditions leading up to a transfer event, including the steady-state likelihood of two cells interacting and any HIV-induced effects on the movement of either cell just prior to a potential transfer. HIV+:HIV+ interactions include this, plus the direct influence of cellular HIV-binding on the formation of interactions. As such, the difference in these measurements reflects the propensity of a HIV+ cell to transfer virus to another specific cell type in its immediate neighborhood. Important to note, HIV+:HIV+ interactions could be in the form of two cells that each have HIV particles, but are not engaged in the process of transfer. As HIV is not influencing the interaction, the frequency of such events would be the same as the steady-state interaction frequency of the cell pair. This frequency is included in the HIV+:HIV- interaction frequency and is therefore accounted for (subtracted) in the 'HIV-transfer phenotype score'.

Association between T cell HIV-load and DC/macrophage interaction

This analysis was performed to determine whether the HIV-load (number of HIV particles) in a CD4+ T cell is associated with increased interactions with either DCs or macrophages (Figure 6E). In particular, CD4+ T cells were split into 4 groups

based on the number of HIV particles they contained (0, 1, 2–3 or $\geq$4 virions). For T cells in each group, their degree of interaction with DCs or macrophages was measured as the number of pixels in the T cell body that belonged to either of these cells (DC: CD11c+ pixels; Macrophage: FXIIIa+ pixels). To account for inter-image variation, we performed all measurements intra-image which meant that a single image was required to have CD4+ T cells with a spectrum of HIV levels to allow for a fair comparison. Accordingly, only images with at least 3 CD4+ T cells in each category (0, 1, 2–3, $\geq$4 virions) were used for the analysis.